University of Alberta

Spectroscopic and *ab initio* Studies of Rare Gas - Formaldehyde van der Waals Complexes

by

Dean Russell Court

A thesis submitted to the Faculty of Graduate Studies and Research in partial fulfillment of the requirements for the degree of Master of Science

Department of Chemistry

Edmonton, Alberta

Fall 2000

National Library of Canada

Acquisitions and Bibliographic Services

395 Wellington Street
Ottawa ON K1A 0N4
Canada

Bibliothèque nationale du Canada

Acquisitions et services bibliographiques

395, rue Wellington
Ottawa ON K1A 0N4
Canada

Your file Votre référence

Our file Notre référence

The author has granted a non-exclusive licence allowing the National Library of Canada to reproduce, loan, distribute or sell copies of this thesis in microform, paper or electronic formats.

L'auteur a accordé une licence non exclusive permettant à la Bibliothèque nationale du Canada de reproduire, prêter, distribuer ou vendre des copies de cette thèse sous la forme de microfiche/film, de reproduction sur papier ou sur format électronique.

The author retains ownership of the copyright in this thesis. Neither the thesis nor substantial extracts from it may be printed or otherwise reproduced without the author's permission.

L'auteur conserve la propriété du droit d'auteur qui protège cette thèse. Ni la thèse ni des extraits substantiels de celle-ci ne doivent être imprimés ou autrement reproduits sans son autorisation.

0-612-59793-8

Canada

University of Alberta

Library Release Form

Name of Author: Dean Russell Court

Title of Thesis: Spectroscopic and *ab initio* Studies of Rare Gas - Formaldehyde van der Waals Complexes

Degree: Master of Science

Year this Degree Granted: 2000

Permission is hereby granted to the University of Alberta Library to reproduce single copies of this thesis and to lend or sell such copies for private, scholarly or scientific research purposes only.

The author reserves all other publication and other rights in association with the copyright in the thesis, and except as herein before provided, neither the thesis nor any substantial portion thereof may be printed or otherwise reproduced in any material form whatever without the author's prior written permission.

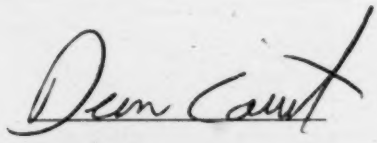

1855 - 37 Street
Edmonton, Alberta, Canada
T6L 3G8

September 27, 2000

ABSTRACT

Rotational spectra of Ar-D_2CO, Ne-H_2CO, and Ne-D_2CO were measured using a pulsed jet cavity Fourier Transform microwave spectrometer. The derived spectroscopic constants were used to derive structural parameters and gain insight into the internal rotation dynamics of the formaldehyde subunit within the complex. Additionally, an *ab initio* study of Ne-H_2CO was carried out to supplement the experimental study of Ne-H_2CO and Ne-D_2CO. Two tunnelling states, due to the interchange of equivalent hydrogen nuclei, were observed for Ar-D_2CO and one tunnelling state for Ne-H_2CO and Ne-D_2CO with neon isotopomers ^{20}Ne and ^{22}Ne. The rare gas-formaldehyde complexes form planar structures with the rare gas atoms nearly perpendicular to the C-O bond of formaldehyde. The deuterium nuclear quadrupole coupling constants confirm that the internal rotation of the formaldehyde subunit is about its C_2 axis in agreement with the smallest barrier to internal rotation calculated from the Ne-H_2CO *ab initio* study.

University of Alberta

Faculty of Graduate Studies and Research

The undersigned certify that they have read, and recommend to the Faculty of Graduate Studies and Research for acceptance, a thesis entitled "Spectroscopic and *ab initio* Studies of Rare Gas - Formaldehyde van der Waals Complexes" submitted by Dean Russell Court in partial fulfillment for the degree of Master of Science.

Supervisor Dr. W. Jäger

Dr. R.E.D. McClung

Dr. J. Tulip

September 27, 2000
Date

Acknowledgement

I wish to thank my supervisor Dr. W. Jäger for all his advice, wisdom, and patience over the years as his graduate student. As well, I would like to thank the other members of the Jäger group, Dr. Yunjie Xu, Silas Ngari, Jennifer van Wijngaarden, and Yaqian Liu, for valuable insights and discussions regarding our area of study. I would also like to thank Dr. Anna Jordan for picking me to be one of her teaching assistant for Chem 27X and for sometimes giving me a different perspective on things.

CONTENTS

CHAPTER ONE

INTRODUCTION 1

CHAPTER TWO

EXPERIMENTAL 5

2.1 FOURIER TRANSFORM MICROWAVE SPECTROMETER 5

2.2 SAMPLE CONDITIONS 9

2.3 MOLECULAR BEAM 11

2.4 BLOCH EQUATION 12

2.5 AB INITIO CALCULATIONS 15

CHAPTER THREE

MOLECULAR SYMMETRY GROUP ANALYSIS 17

3.1 INTRODUCTION 17

3.2 ANALYSIS 17

3.2.1 ANALYSIS OF RG-H_2CO 17

3.2.2 ANALYSIS OF RG-D_2CO 22

3.2.3 NUCLEAR QUADRUPOLE ANALYSIS 26

CHAPTER FOUR

Ar-D_2CO 28

4.1 INTRODUCTION 28

4.2 EXPERIMENTAL 29

4.3 SPECTRAL SEARCH AND ASSIGNMENT 29

4.4 ANALYSIS, RESULTS AND DISCUSSION 34

4.4.1 IDENTIFICATION OF STATES 34

4.4.2 STRUCTURE DETERMINATION 37

4.4.3 NUCLEAR QUADRUPOLE COUPLING 38

4.5 CONCLUSIONS 41

CHAPTER FIVE

ROTATIONAL SPECTRA OF THE Ne-H_2CO AND Ne-D_2CO COMPLEXES 42

5.1 INTRODUCTION 42

5.2 EXPERIMENTAL 43

5.3 SPECTRAL SEARCH AND ASSIGNMENT 44

5.4.1 IDENTIFICATION OF THE STATE 52

5.4.2 STRUCTURE DETERMINATION 55

5.4.3 NUCLEAR QUADRUPOLE COUPLING 56

5.5 CONCLUSIONS 59

CHAPTER SIX

AB INITIO CALCULATIONS ON Ne-H_2CO 60

6.1 INTRODUCTION 60

6.2 EXPERIMENTAL 60

6.2.1 SUPERMOLECULAR APPROACH 60

6.2.2 COUNTERPOISE CORRECTION 61

6.3 BASIS SETS 61

6.3.1 ATOMIC BASIS SETS 61

6.3.2 BOND FUNCTIONS 62

6.3.3 GEOMETRIES 63

6.4 RESULTS AND DISCUSSION 64

6.4.1 GLOBAL MINIMUM 64

6.4.2 TUNNELLING PATHWAYS 68

6.5 CONCLUSIONS 73

CHAPTER SEVEN

CONCLUSIONS 74

BIBLIOGRAPHY

BIBLIOGRAPHY 76

List of Tables

3.1 Character table of the Molecular symmetry C_{2v}(M) group for Rg-H_2CO 18

3.2 Spin orientation under symmetry group operations for Rg-H_2CO 22

3.3 Spin orientation under symmetry group operations for Rg-D_2CO 26

4.1 Measured ground tunnelling states transitions of Ar-D_2CO 31

4.2 Measured first excited tunnelling state transitions of Ar-D_2CO 33

4.3 Determined Rotational, centrifugal distortion and Deuterium Quadrupole coupling constants of Ar-D_2CO 35

4.4 Calculated and Experimental nuclear quadrupole coupling constants of Ar-D_2CO 40

5.1 Measured Ground Tunnelling State Transitions for Ne-H_2CO 45

5.2 Possible Transitions for Ne-H_2CO 46

5.3 Measured Ground Tunnelling State Transitions for Ne-D_2CO 48

5.4 Possible Transitions for Ne-D_2CO 49

5.5 Well Determined Constants for Ne-H_2CO 52

5.6 Determined Constants for Ne-D_2CO 52

5.7 Well Determined Constants of Ne-D_2CO 53

5.8 Determined Constants of Ne-D_2CO 53

5.9 Calculated and Experimental Quadrupole Coupling Constants for Ne-D_2CO 57

6.1 Calculated *ab initio* energies of Ne-H_2CO 65

6.2 Barriers to the tunnelling motions of Ne-H_2CO 72

List of Figures

2.1 The mechanical parts of the Fourier Transform Microwave Spectrometer 6

2.2 The schematic of the microwave circuitry used by the spectrometer 7

2.3 Timing diagrams used in a single experiment 10

3.1 Molecular symmetry group operations for Rg-H_2CO 18

3.2 Molecular symmetry group operations for Rg-D_2CO 24

4.1 1_{01}-0_{00} spectra of Ar-D_2CO showing both tunnelling states with deuterium hyperfine 36

4.2 Determined structures of Ar-H_2CO 39

5.1 Predicted structure of Ne-H_2CO 45

5.2 1_{01}-0_{00} spectra of Ne-D_2CO showing both tunnelling states with deuterium hyperfine 47

5.3 Determined structure of Ne-H_2CO 56

6.1 Potential energy surface of Ne-H_2CO at dihedral angle of 0° 69

6.2 Inplane tunnelling minimum energy pathways 70

6.3 Out of plane tunnelling minimum energy pathway 71

CHAPTER ONE

INTRODUCTION

The properties of a system of interacting entities are determined by the properties of the individual entities and the exact nature of their interaction. An example is the interactions between animals, plants and the environment. An entire field, namely ecology, exists for the purpose of studying these interactions. As the systems under consideration become smaller, many other areas of study arise. The study of interactions between people is known as sociology. Still, as the field of view narrows further, the study of interactions within an organism belongs to the field of biology. Interactions inside a cell within an organism are studied within the field of molecular biology. In the end, the study of the most basic interactions, those between molecules and atoms, belongs to the field known as physical chemistry.

Interactions between molecules can be classified into two categories, long range and short range interactions.[1,2] The origin of the long range attractive interactions are electrostatic, induction and dispersion forces. The electrostatic force results from the Coulombic interaction between the permanent electric multipole moments of the involved molecules. Induction interaction arises when the electric field of a polar molecule distorts the electronic charge distribution of a neighbouring molecule. The induced moment can then interact with the inducing multipole moment. The dispersion contribution originates from a correlation of the fluctuating electronic charge distribution of the binding partners. At any time there may exist an instantaneous dipole moment that can, in turn, induce a moment in another atom, leading to an attractive force.

The short range repulsive interaction is a result of the Pauli exclusion principle. If two closed shell molecules approach, the electron density in the overlap region is reduced. The nuclei are then deshielded and repel each other.

In the present case, the study of formaldehyde containing van der Waals complexes with rare gas atoms, the main long range intermolecular force is dispersion. Formaldehyde is a polar molecule, but the van der Waals complexes are formed with rare gas atoms, so an electrostatic interaction will not be present. The induction intermolecular force will be present, but its contribution is, in general, small compared to the electrostatic and dispersion forces.

One goal of the study of weakly bound complexes, like, for example, rare gas - formaldehyde, is the determination of the interaction potential energy surface. The potential energy surface is a multidimensional representation of the interaction energy as a function of separation and orientation of the constituent monomers. Measurement of bulk phase properties, such as viscosity and thermal conductivity, is one important way to obtain information about weak interactions. The determined quantities, however, represent averages over a range of separations and orientations, and are also contaminated by three- and more-body interactions. High resolution spectroscopy of van der Waals complexes can separate out two and more-body interaction by investigating dimer, trimer, and larger systems individually. Furthermore, spectra of van der Waals complexes depend very sensitively on the particular interaction potential energy surface. The inversion of transition frequencies or the resulting spectroscopic parameters, such as rotational and centrifugal distortion constants, to potential energy surface parameters is, however,

extremely difficult.

An intimate interplay of theoretical and experimental methods is necessary to tackle this problem. *ab initio* methods, for example, have become powerful enough in recent years to determine intermolecular interaction energies for small systems with sufficient accuracy. Methods have also become available in recent years to determine bound state ro-vibrational energy levels that are supported by, for example, *ab initio* potential energy surfaces.[3,4,5] One approach is then to compare calculated transition frequencies with the experimental ones. If the differences are significant, the *ab initio* surface can be scaled until a satisfactory agreement is achieved.

This thesis deals with formaldehyde containing van der Waals complexes, specifically, Ar-D_2CO, Ne-H_2CO and Ne-D_2CO. Formaldehyde is an ideal compound to be used in the study of van der Waals complexes. The structure of the formaldehyde monomer is well determined,[6,7,8,9] leaving any ambiguity about the formaldehyde monomer in the complex behind. Formaldehyde is the simplest molecule containing the carbonyl functional group and an understanding of its interaction with rare gas atoms provides a starting point for the study of the role of the carbonyl group in more complex systems.

This thesis is broken down into three major parts: theory and experimental setup, experimental results, and *ab initio* results. The theory and experimental setup is presented in two chapters. Chapter two deals with the experimental setup of the Fourier transform microwave spectrometer used. Also in Chapter two is some of the basic theory behind molecular beams and the Bloch equations as well as the type of *ab initio* calculation performed. Chapter three presents the molecular symmetry group analysis for all

Rg-H_2CO and Rg-D_2CO complexes. The next major section, experimental results, is also presented in two chapters. Chapter four deals with the experimental results of Ar-D_2CO, a continuation of a study on Ar-H_2CO[10] with additional information supplied from the deuterium nuclear quadrupole hyperfine structure of fully deuterated formaldehyde. Chapter five presents partial experimental results for Ne-H_2CO and Ne-D_2CO. These van der Waals complexes display increased floppiness as compared to their Ar-H_2CO analogs. As well, additional information from the deuterium nuclear quadrupole hyperfine structure of the transitions of fully deuterated neon-formaldehyde is collected. The last major section, *ab initio* results, is presented in Chapter six. A full potential energy surface including barriers to the internal rotation of the formaldehyde subunit within the complex was determined. Chapter seven presents conclusions based on the work done for this thesis.

CHAPTER TWO

EXPERIMENTAL

2.1 FOURIER TRANSFORM MICROWAVE SPECTROMETER

The instrument[11] used for studying the van der Waals complexes is a molecular beam Fourier Transform microwave spectrometer[12] of the Balle-Flygare type.[13] The sample cell of the spectrometer is a Fabry-Perot microwave cavity situated inside a vacuum chamber. The chamber is pumped by a 30cm diffusion pump backed by a 2000 ls^{-1} mechanical pump. The vacuum chamber can be easily opened by having one end flange on rollers, allowing access to the microwave cavity. The cavity consists of two spherical aluminum mirrors having a diameter of 26cm and a radius of curvature of 38cm. One mirror is mounted onto the movable end flange of the vacuum chamber, the other mirror can be adjusted using a computer controlled DC actuator. The adjustable mirror can be moved to tune the microwave cavity into resonance with the external microwave radiation. A microwave antenna is mounted in the middle of the fixed aluminum mirror. The antenna acts as both microwave transmitter and receiver and is attached to the microwave circuitry outside of the vacuum chamber. A pulsed nozzle (General Valve, Series 9) with 0.8mm nozzle orifice diameter is also mounted in the fixed mirror near the centre of the mirror.[14] The pulsed nozzle is attached to a sample system through copper tubing. The arrangement of the pulsed nozzle with respect to the microwave cavity gives a molecular expansion being parallel to the cavity axis. Figure 2.1 shows a schematic of the vacuum chamber and microwave cavity.

A Hewlett Packard microwave synthesizer with a frequency range of 1-20 GHz

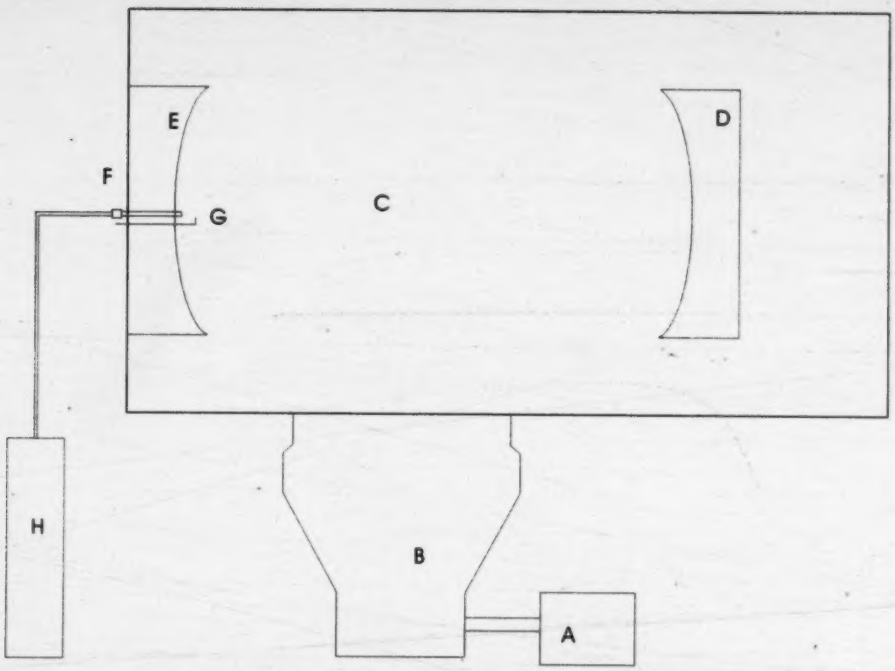

Figure 2.1: A schematic representation of the mechanical parts of the Fourier Transform microwave spectrometer. The microwave cavity (C) is pumped by a diffusion pump (B) backed by a mechanical pump (A). The microwave cavity is formed by a fixed mirror (E) and a movable mirror (D). The microwave radiation is introduced into the cavity through an antenna (G). The sample is pulsed into the chamber using a pulsed solenoid valve (F) from a sample reservoir (H).

generates coherent microwave radiation. A schematic of the microwave circuitry is shown in Figure 2.2. The microwave radiation emitted by the synthesizer is 20 MHz below the desired excitation frequency. The microwave radiation, after passing through an isolator, is split into two components, one for use in the detection system, the other for the excitation pulse. An isolator allows microwave radiation to flow in only one direction. The purpose of an isolator is to prevent feedback of microwave radiation, thereby protecting sensitive microwave components. The microwave excitation pulse is formed by

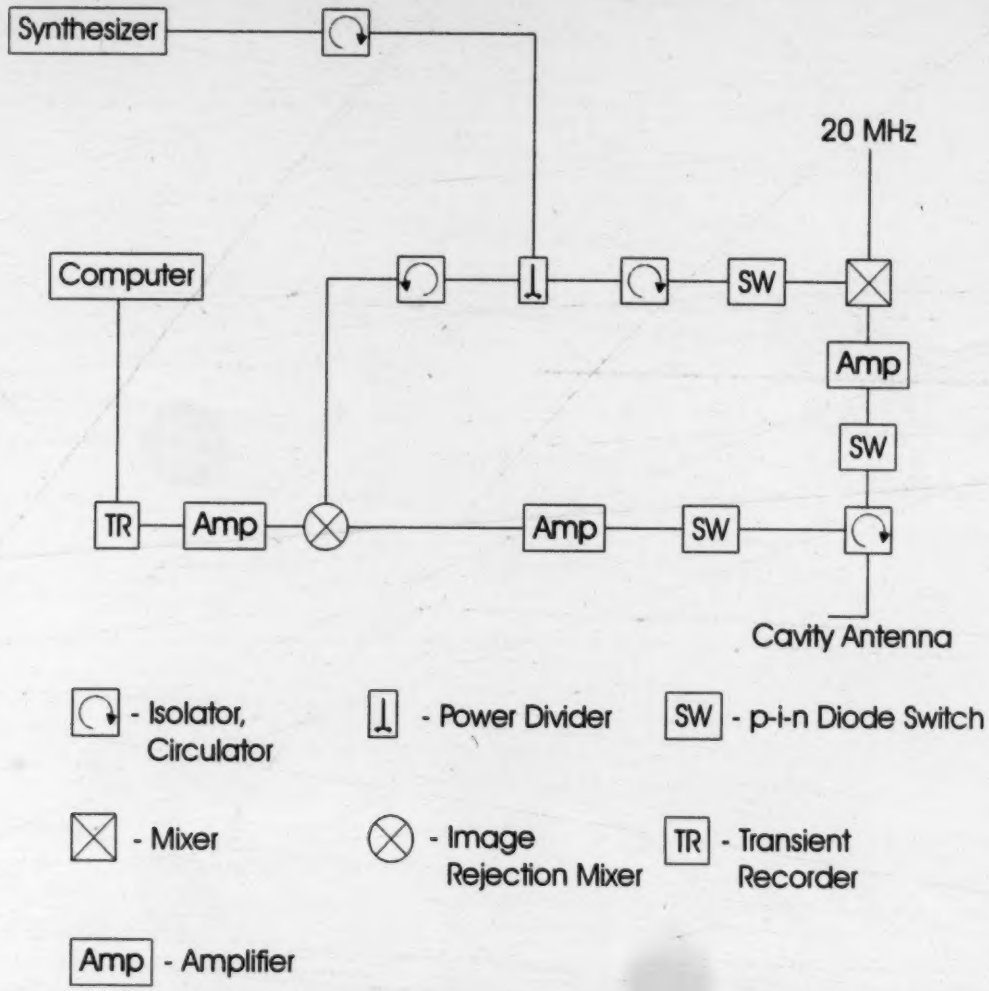

Figure 2.2: The schematic of the microwave circuitry of the molecular beam Fourier Transform microwave spectrometer. The synthesizer generates the desired microwave frequency less 20MHz. The coherent microwave radiation is split into two paths, one for the superheterodyne detection circuit, the other for the microwave excitation pulse. The microwave radiation for the excitation pulse is mixed with 20MHz to get the desired frequency then amplified before being introduced into the microwave cavity. The molecular emission signal from the microwave cavity is amplified and mixed down to radio frequencies around 20MHz. The time domain signal is recorded with a transient recorder and stored in the computer for signal averaging.

a p-i-n diode switch then fed into a microwave mixer. The switch is utilized to attenuate the microwave radiation by about 30dB. The mixer is fed with a 20 MHz IF signal. From the mixer, two different microwave frequencies are produced, one that is 20 MHz greater than the synthesizer frequency, the other is 20 MHz lower than the synthesizer frequency. The higher frequency is the frequency that is desired. The microwave radiation then passes through an optional solid state amplifier (if required to increase the power of the microwave radiation). The microwave radiation passes through another p-i-n diode switch then a 3-way circulator. The microwave excitation radiation is then emitted from a wire hook antenna into the microwave cavity. The molecular emission is picked up by the same antenna, passes through the 3-way circulator and into a superheterodyne detection system. The detection system is protected by a third p-i-n diode switch and has a low noise microwave amplifier on the front end. The microwave signal is combined with the original microwave synthesizer radiation at the image rejection mixer to obtain a down converted signal at around 20 MHz. The time domain signal is then recorded with a transient recorder and the data is transferred to a computer for Fourier transformation. Data is recorded every 20ns for nominal resolution to 60ns or 120ns for high resolution spectra. The number of data points collected is 4096. For the Fourier transformation, an additional 4096 zero data points are added at the end of the data set and then transformed.

A single experiment can be broken down into several phases: a molecular pulse, a molecule-microwave delay, a microwave pulse, an additional delay and an observation period. The experiment starts by first introducing a molecular pulse into the cavity. The duration of the molecular pulse is on the order of a millisecond. A short delay of about a

millisecond follows before the microwave excitation pulse is introduced into the cavity. The microwave excitation pulse is generated by opening the p-i-n diode switch for typically a few microseconds. A delay between the end of the microwave excitation pulse and the beginning of the sampling period is on the order of a few micro seconds. The detection protective switch remains closed from the beginning of the experiment until the end of the delay period. The molecular signal is sampled every 20ns for nominal resolution or 120ns for high resolution, collecting 4096 data points. At the end of the experiment, all protective switches close. A background signal is also recorded for every experiment. The background signal is subtracted from the molecular signal. The background signal is recorded in exactly the same manner as the molecular signal, except that there is no molecular pulse. Figure 2.3 shows the timing diagram for both molecular and background signals. To ensure that the background subtraction is phase synchronous, a reference signal of 10 MHz from the synthesizer is used as the master clock for the timing sequence.

To increase the signal to noise ratio, additional experiments can be done. The signal of each new experiment is added to the previous signal(s); this is called signal averaging. This is possible since all the previous signals and any new signal will be in phase by referencing all timing pulses to the 10MHz clock of the synthesizer. At any point, the averaged signal can be Fourier transformed and the power spectrum viewed graphically.

2.2 SAMPLE CONDITIONS

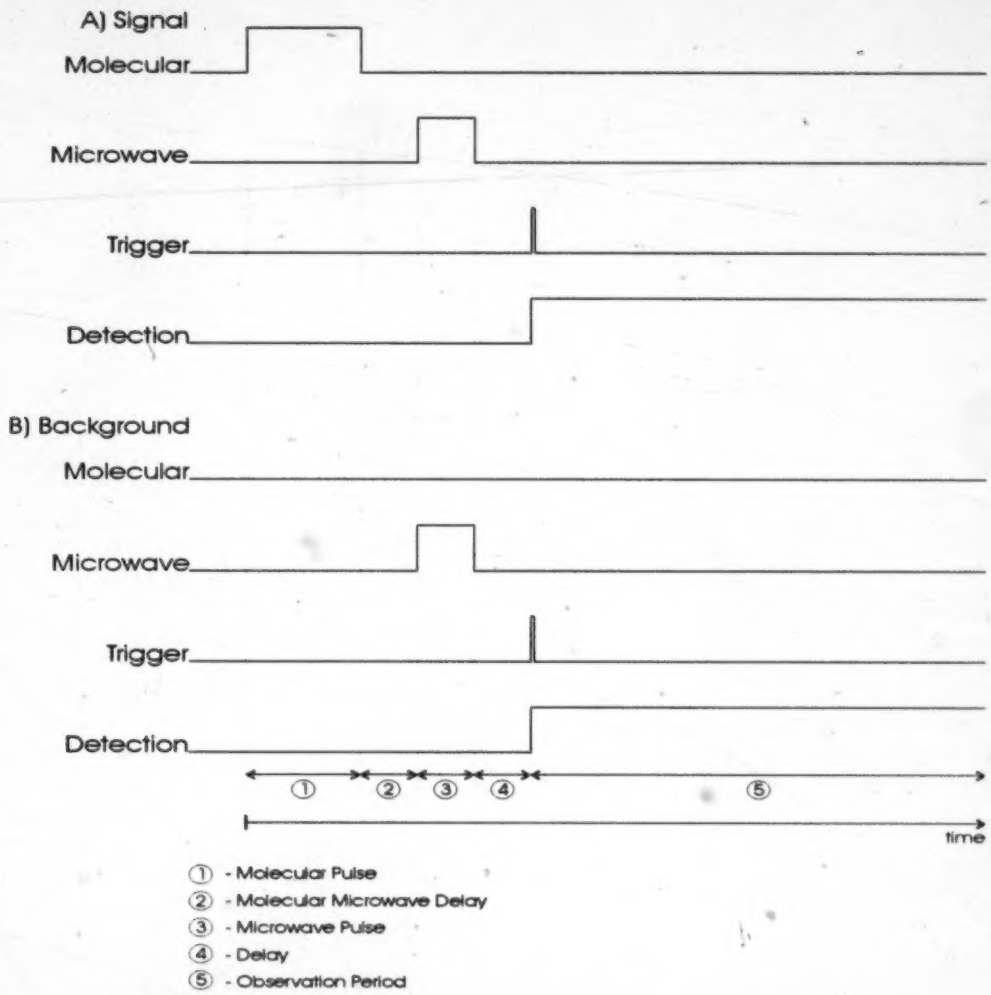

Figure 2.3: A timing diagram for one experiment with (A) and without (B) the molecular beam. "Molecular" refers to the opening and closing of the solenoid valve connected to the sample system. "Microwave" refers to the period in which microwave radiation is introduced into the microwave cavity. "Trigger" refers to the signal that starts the recording of the time domain signal. "Detection" refers to the switch after the microwave cavity in detection circuit in which the signal is recorded. Each experiment consists of two separate microwave pulses, one with the molecular pulse and the other without. A) refers to the microwave pulse with the molecular beam present, while B) refers to the microwave pulse without the molecular beam present. The signal from B) is subtracted from the signal from A).

The sample conditions used to characterize the van der Waals complexes Ar-H_2CO and Ar-D_2CO spectroscopically were 4% argon and 0.4% H_2CO or D_2CO with neon as backing gas at a total pressure of 3.2 atm. Sample conditions used to characterize Ne-H_2CO and Ne-D_2CO were 0.4% H_2CO or D_2CO with neon backing gas at a total pressure of 3.2 atm. The entire sample system was heated with heating tape to prevent the formaldehyde from condensing back into paraformaldehyde.

2.3 MOLECULAR BEAM

The sample is introduced into the vacuum chamber using the pulsed nozzle. The gas from the nozzle expands into the vacuum chamber, thereby cooling the van der Waals complexes. The expansion from the nozzle changes the random motion of the static gas in the sample system into directed mass flow in the vacuum chamber.[15] In the experiments carried out, the molecular expansion is a supersonic free jet expansion. It is a supersonic free jet expansion due to the fact that the sample pressure is much greater than twice the background pressure in the vacuum chamber and nothing in the vacuum chamber interferes with how the molecular pulse expands.

The mass flow of each nozzle pulse resembles that of neon since the amount of formaldehyde in the sample is small. As a consequence of this, formaldehyde and argon are accelerated to the velocity at which neon travels in the molecular expansion.[16] The translational temperature corresponds to the velocity distribution of all molecules in the sample. A directed mass flow occurs when a small portion of the sample is pulsed into the vacuum chamber through the nozzle giving a molecular expansion with a uniform velocity

distribution. This results in a low translational temperature due to the narrow velocity distribution. By using a directed mass flow, the translational degrees of freedom are restricted[17] and a low translational temperature molecular beam results.

The molecular pulse, which is mostly neon carrier gas, acts like a cooling bath for other compounds and complexes in the expansion. The other degrees of freedom, vibrational and rotational, are cooled through collisions as the molecular pulse expands. The cooling occurs rapidly after the pulse leaves the nozzle through collisions, but the number of collisions drops off as the molecular pulse expands. The amount of cooling is limited by the static sample pressure and the diameter of the nozzle.[18] The number of collisions is increased by increasing the static sample pressure and by increasing the diameter of the nozzle. Rotational cooling is more efficient than vibrational cooling as each collision removes an amount of energy closer to the rotational rather than the vibrational energy level spacing. Thus many more collisions are required to cool the vibrational degrees of freedom to the same degree as the rotational degrees of freedom.[16] In the Fourier Transform microwave spectrometer used, the rotational temperature is estimated to be on the order of 1 °K.

2.4 BLOCH EQUATION

For a signal to be detected in Fourier Transform microwave spectroscopy, four main conditions must be met. The first condition is that the frequency of the microwave excitation pulse is close to a transition frequency. The second condition that is required for a transition between two levels to be detected is that there is a transition dipole

moment between the two levels. In a simplistic system with only two levels the time dependent Hamiltonian[19,20,21] is:

$$H=\begin{pmatrix} H_{aa} & H_{ab} \\ H_{ba} & H_{bb} \end{pmatrix}=\begin{pmatrix} E_a & -2\mu_{ab}\varepsilon\cos\left[\omega\left(t-t_0\right)-kz\right] \\ -2\mu_{ab}\varepsilon\cos\left[\omega\left(t-t_0\right)-kz\right] & E_b \end{pmatrix} \qquad (2.1)$$

where E_a and E_b are the energies of the two levels involved, μ_{ab} is the matrix element of the dipole operator $\hat{\mu}$, 2ε is the electric field strength, ω is the frequency of the microwave radiation, k is the frequency ω divided by the speed of light in a vacuum, z is the translational coordinate for which the dipole interaction is considered and $(t-t_0)$ is the time since the microwave pulse was applied. If μ_{ab} is zero, no electric dipole transition will be seen.

The third condition is that there must be a non-zero population difference between the two levels of interest. The molecular expansion creates a population difference between levels due to the low rotational temperature in the beam. The populations N_a and N_b of the levels with energies E_a and E_b, respectively, follow the Boltzmann distribution:

$$\frac{N_a}{N_b}=\exp-\left(E_a-E_b\right)/kT \qquad (2.2)$$

where k is the Boltzmann constant, and T is the rotational temperature. For a transition frequency of 10GHz at 1°K, the ratio N_a/N_b is 0.618. As the temperature increases, this ratio decreases markedly.

The final condition that must be met to achieve a maximum signal is the $\frac{\pi}{2}$ excitation pulse condition. An analogy can be drawn between Fourier Transform Nuclear Magnetic Resonance spectroscopy and Fourier Transform microwave spectroscopy. The

Bloch equations[22] describe the interaction of an ensemble of magnetic dipoles with electromagnetic radiation while the optical analogues[19] deal with the interaction of an ensemble of electric dipoles with electromagnetic radiation. Without going through the entire derivation, the important Bloch equation analogues are:

$$\begin{aligned} &\frac{\partial P_i}{\partial t}+\left(\omega_0-\omega\right)P_i=0 \\ &\frac{\partial P_i}{\partial t}-\left(\omega_0-\omega\right)P_r+\chi^2\varepsilon\frac{\hbar}{4}\Delta N=0 \\ &\frac{\hbar}{4}\chi\frac{\partial\Delta N}{\partial t}-\chi\varepsilon P_i=0 \end{aligned} \tag{2.3}$$

where P_i and P_r are the in and out of phase components of the polarization of the molecular ensemble, ω_0 is the transition frequency, ω is the frequency of the microwave excitation pulse, χ is equal to $\frac{2\mu_{ab}}{\hbar}$, ΔN is the population difference between the two levels, ΔN_0 is the initial population difference and ε is microwave electric field strength. The equations presented ignore relaxation terms. Solutions to equations (2.3) for the microwave excitation period can be found by assuming that the term involving the microwave field strength is much larger than the off resonance term, and assuming that $\omega_0 - \omega = 0$. The critical conditions at time $t = t_0$ are:

$$\begin{aligned} &P_r(t_0)=P_i(t_0)=0 \\ &\Delta N(t_0)=\Delta N_0 \end{aligned} \tag{2.4}$$

The polarization, $\left(P_r(t)^2+P_i(t)^2\right)^{\frac{1}{2}}$, at time t is a maximum when:

$$\chi\varepsilon\left(t-t_0\right)=(2n+1)\frac{\pi}{2} \tag{2.5}$$

provided $\omega_0 - \omega \approx 0$. When n is zero, this is the $\frac{\pi}{2}$ condition that must be met in order to maximize the detected signal. The solutions to the Bloch equations (2.3) under the resonance conditions are:

$$P_r(t)=0$$
$$P_i(t)=-\frac{\hbar\chi^2\varepsilon\Delta N_0}{4\chi\varepsilon} \qquad (2.6)$$
$$\Delta N(t)=0$$

Under the $\frac{\pi}{2}$ microwave pulse conditions at resonance, the maximum polarization is in phase and there is no out of phase polarization. The interpretation of this is that the ensemble of molecules are rotating coherently. If these four conditions are met, it is possible for a microwave signal to be detected.

2.5 AB INITIO CALCULATIONS

ab initio calculations were performed on the Ne-H_2CO van der Waals complex. The level of the theory was second and fourth order Møller-Plesset perturbation theory[23] (MP2 and MP4). The program used for the calculations was Gaussian 94[24,25] and the computers used for the calculations included a 16-node Beowulf cluster (Pentium III - 500 MHz/512Mb), a Pentium III - 450 MHz/512Mb and a Pentium II - 266 MHz/256Mb. The basis sets used were Dunning's aug-cc-pVTZ[26] for Ne and Sadlej's pVTZ[27] for C, O and H. A set of bond functions[28,29,30,31] was supplemented midway between the Ne atom and the centre of mass of the formaldehyde monomer.

The geometry used for H_2CO was derived from a geometry optimization using MP2 and MP4 level of theory. For calculations at the MP2 level, the H_2CO geometry optimized at the MP2 level was used and the MP4 optimized geometry for calculations at the MP4 level. The structure of the H_2CO monomer was frozen in all calculations.

The orientation of the neon atom with respect to the formaldehyde monomer can

be described by three coordinates, a radial coordinate R which is the distance from the centre of mass of the H_2CO monomer to the Ne atom, an angle θ formed by the oxygen, formaldehyde centre of mass and the neon atom. The last coordinate, Φ, is the angle (out of plane) formed by the intersection of two planes: the formaldehyde plane and the plane formed by formaldehyde's oxygen and centre of mass and the neon atom. The supermolecular approach[32] was used in the calculations. Equation (2.7) describes the general method.

$$\Delta E_{AB} = E_{AB} - E_A - E_B \qquad (2.7)$$

ΔE_{AB} is the interaction energy between the two monomers; in the present case, H_2CO is one monomer and Ne is the other monomer. E_{AB}, E_A and E_B refer to the absolute energy of the dimer and each monomer respectively. Each monomer energy is calculated with the full dimer basis set present, except that the nuclear charge of the other monomer is set to zero. This style of calculation is called the counterpoise correction[33]. The error that is corrected by the counterpoise correction is called the basis set superposition error.

CHAPTER THREE

MOLECULAR SYMMETRY GROUP ANALYSIS

3.1 INTRODUCTION

The presence of two or more identical nuclei in a molecular system can have profound effects on its spectrum if these nuclei can be interchanged through some internal motion. In rare gas - formaldehyde complexes (Rg-H_2CO), for example, the two equivalent hydrogen nuclei can be interchanged through an internal rotation motion of the formaldehyde subunit about its symmetry axis. The two symmetrically equivalent forms of Rg-H_2CO are separated by a barrier to this internal rotation motion. The possibility of tunnelling between the two structures through the barrier leads to a splitting of ro-vibrational energy levels, and a tunnelling splitting can be observed in the spectra. In order to properly label the energy levels and to predict and to interpret the spectrum, a molecular symmetry group analysis[34] was done.

3.2 ANALYSIS

3.2.1 ANALYSIS OF RG-H_2CO

The molecular symmetry group of the Rg-H_2CO consists of the following nuclear permutation inversion operations: E, (12), E^*, $(12)^*$ and is called $C_{2V}(M)$. E is the identity operation, (12) refers to the interchange of H_1 and H_2, E^* refers to an inversion of all molecular coordinates through the centre of mass of the complex, and $(12)^*$ is an interchange of H_1 and H_2 followed by an inversion of all molecular coordinates. Figure 3.1 shows the effects of the various operations[34] on Rg-H_2CO. Table 3.1 shows the character

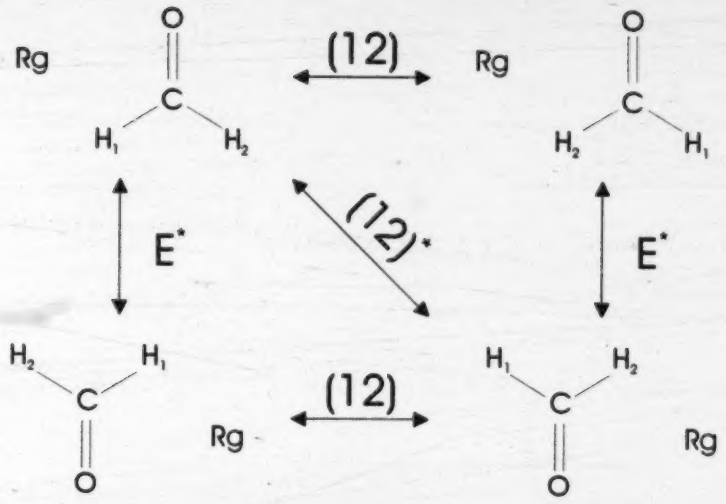

Figure 3.1: The molecular symmetry group operations for Rg-H_2CO van der Waals complexes. (12) refers to the interchange of H_1 and H_2. E^* refers to the complete inversion of all molecular coordinates through the centre of mass. $(12)^*$ refers to the interchange of H_1 and H_2 followed by an inversion of all molecular coordinates through the centre of mass.

Table 3.1: Character Table for the Molecular Symmetry Group $C_{2V}(M)$ for Rg-H_2CO van der Waals Complexes.

	E	R_{tun} (12)	R_c^π E^*	$R_{tun}R_c^\pi$ $(12)^*$
A_1	1	1	1	1
A_2	1	1	-1	-1
B_1	1	-1	-1	1
B_2	1	-1	1	-1

table for the $C_{2v}(M)$ molecular symmetry group. The $C_{2v}(M)$ molecular symmetry group is isomorphic to the C_{2v} point group and their character tables are the same. Also included in Table 3.1 are the equivalent rotations that correspond to the nuclear permutation inversion operations. The equivalent rotations are combinations of rotations of the complex about its principal inertial axis and of internal tunnelling motions. For example, E* is equivalent to a rotation about the c-axis by 180°, denoted by R_c^{π}. (12) is equivalent to the tunnelling motion, that is, an internal rotation of the formaldehyde subunit about its symmetry axis and is denoted as R_{tun}.

The next step is the symmetry classification of the molecular wave function under the operations of the molecular symmetry group. Spin statistical laws govern the symmetry behaviour of the total wave function if identical nuclei are exchanged, such as the two hydrogen nuclei in Rg-H_2CO. Nuclei with half integer spin, such as protons (spin I = ½) are called Fermions and obey Fermi-Dirac statistics. An exchange of two identical Fermions requires the total molecular wave function to change sign[35] (Pauli exclusion principle). Nuclei with integer spin, for example the deuterium nucleus (spin I = 1), obey Bose-Einstein statistics. If two equivalent Bosons are exchanged, the sign of the molecular wave function is unaffected.

For the following symmetry considerations, we assume that the total wave function Ψ_{tot} can be written as the product of electronic, Ψ_{el}, vibrational, Ψ_{vib}, rotational, Ψ_{rot}, tunnelling, Ψ_{tun}, and nuclear spin, Ψ_{spin}, wave functions.:

$$\Psi_{tot} = \Psi_{el}\Psi_{vib}\Psi_{rot}\Psi_{tun}\Psi_{spin} \qquad (3.1)$$

Accordingly, the symmetry behaviour of the total wave function under the operations of

the $C_{2v}(M)$ molecular symmetry group can be written:

$$\Gamma_{tot} = \Gamma_{el} \otimes \Gamma_{vib} \otimes \Gamma_{rot} \otimes \Gamma_{tun} \otimes \Gamma_{spin} \qquad (3.2)$$

where the Γ's are the representations of the corresponding wave functions. The representation of the total wave function Γ_{total} is $B_1 \oplus B_2$. This is found from the symmetry behaviour under the operation (12) (see Table 3.1). When the two hydrogens are interchanged, the wave function must change sign since the hydrogens are fermions.[35] Under the operation (12), the only representations that satisfy this requirement are B_1 and B_2 as A_1 and A_2 do not change sign under (12).

The Rg-H_2CO complex has a $^1\Sigma$ electronic configuration and the electronic wave function belongs to the totally symmetric, A_1, representation. All rotational transitions under consideration in this work occur in the vibrational ground state. The ground state vibrational wave function transforms as the totally symmetric, A_1, representation. The representation for the rotational wave function can be found by examining the symmetry behaviour under operations that contain equivalent rotations R_a^π, R_b^π and R_c^π.[34] The only rotation involved here is R_c^π and the symmetry of the rotational wave function depends only on the quantum number K_c. The two operations that involve R_c^π are E^* and $(12)^*$. For even K_c, the wave function does not change sign under these operations, and the rotational wave function belongs to the A_1 representation. For odd K_c, the rotational wave function changes sign under those operations, and it belongs to the A_2 representation.

The representation for the tunnelling wave function can be found in a similar manner. The tunnelling motion is involved with the operations (12) and $(12)^*$. In the

ground tunnelling state, the tunnelling wave function does not change sign under these operations and belongs to the totally symmetric, A_1, representation. In the first excited tunnelling state, it changes sign and belongs to the B_2 representation.

The hydrogens of formaldehyde have spin ½ and their orientation can be either up (+½) or down (-½). To determine the nuclear spin wave function representation, the different permutations of spin orientation are tested under the symmetry group operations. Table 3.2 shows the different spin orientations and the result under each symmetry group operation. The spin wave function representation for all spin orientations decomposes into $3A_1 \oplus B_2$.

After the symmetry representation of the various parts of the total wave function are found one can determine which representation of rotational, tunnelling and nuclear spin parts can be combined to give the right symmetry, i.e. B_1 or B_2, of the total wave function. For the tunnelling ground state:

$$\Gamma_{total} = \Gamma_{elec}\Gamma_{vib}\Gamma_{rot}\Gamma_{tun}\Gamma_{spin}$$

$$A_1 \otimes A_1 \otimes \begin{pmatrix} A_1 \\ A_2 \end{pmatrix} \otimes A_1 \otimes (3A_1 \oplus B_2) = \begin{pmatrix} B_2 \\ B_1 \end{pmatrix} \oplus \begin{pmatrix} 3A_1 \\ 3A_2 \end{pmatrix} \qquad (3.3)$$

In the tunnelling ground state, rotational wave functions with the even K_c, i.e. with A_1 symmetry, can only combined with nuclear spin functions of B_2 symmetry to give a B_2 symmetry for the total wave function. The spin weight of these rotational levels are one. Rotational wave functions with odd K_c (A_2 symmetry) can also combine with nuclear spin functions of B_2 symmetry to give total symmetry B_1.

A similar analysis for the first excited tunnelling state reveals the following:

Table 3.2: Spin Orientation under Symmetry Group operations for Rg-H_2CO.

H_1	H_2	E	-12	E^*	$(12)^*$
α	α	1	1	1	1
α	β	1	0	1	0
β	α	1	0	1	0
β	β	1	1	1	1
	Σ	4	2	4	2

α - spin up, β - spin down

$$\Gamma_{total} = \Gamma_{elec}\Gamma_{vib}\Gamma_{rot}\Gamma_{tun}\Gamma_{spin}$$

$$A_1 \otimes A_1 \otimes \begin{pmatrix} A_1 \\ A_2 \end{pmatrix} \otimes B_2 \otimes (3A_1 \oplus B_2) = \begin{pmatrix} 3B_2 \\ 3B_1 \end{pmatrix} \oplus \begin{pmatrix} A_1 \\ A_2 \end{pmatrix} \qquad (3.4)$$

Here, rotational wave functions with even (odd) K_c, i.e. A_1 (A_2) symmetry, can combine with A_1 nuclear spin functions to give a total wave function with B_2 (B_1) symmetry. The spin weight of levels in the excited tunnelling state is three. Since electric dipole transitions are not allowed between levels with spin functions of different symmetry, only rotational transitions within each tunnelling state are allowed. Furthermore, since nuclear spin conversion is not allowed in the molecular beam expansion, the excited tunnelling state is metastable and its rotational levels are populated such that rotational spectra can be observed.

3.2.2 ANALYSIS OF RG-D_2CO

A similar type of analysis can be done for Rg-D_2CO van der Waals complexes.

Figure 3.2 shows the various permutation inversion operations[34] on Rg-D_2CO similar to that shown in Figure 3.1 for Rg-H_2CO. Again as in Figure 3.1, E is the identity operation, (12) refers to the interchange of D_1 and D_2, E^* refers to an inversion all molecular coordinates through the centre of mass of the complex and $(12)^*$ is an interchange of D_1 and D_2 followed by an inversion of all molecular coordinates. This complex also follows the same molecular symmetry group $C_{2V}(M)$ character table as Rg-H_2CO shown in Table 3.1. The analysis is identical to the analysis done for Rg-H_2CO with a few exceptions. The nuclear spin statistics follow Bose-Einstein statistics which affects the representation of the total wave function and the representation of the nuclear spin wave function.

The two equivalent deuterium nuclei in Rg-D_2CO have nuclear spin I = 1, and are bosons. The system obeys the Bose-Einstein statistics which require that the sign of the total wavefunction remain unchanged under exchange of the two deuterium nuclei. From Table 3.1, it can be seen that representation A_1 and A_2 remain unchanged under the (12) operation which corresponds to the tunnelling motion R_{tun}.

The Rg-D_2CO complex has the same $^1\Sigma$ electronic configuration as Rg-H_2CO and as such, the electronic wave function representation belongs to A_1. Again, as with Rg-H_2CO, the rotational transitions under consideration occur in the vibrational ground state. The representation of the vibrational wave function is A_1. The representation of the rotational wave function is the same as Rg-H_2CO. The symmetry of the rotational wave function is determined from the only rotation involved, R_c^{π}, which is determined from the two operations E^* and $(12)^*$. The symmetry will only depend on the quantum number K_c. For even K_c, the wave function does not change sign under these operations, and the

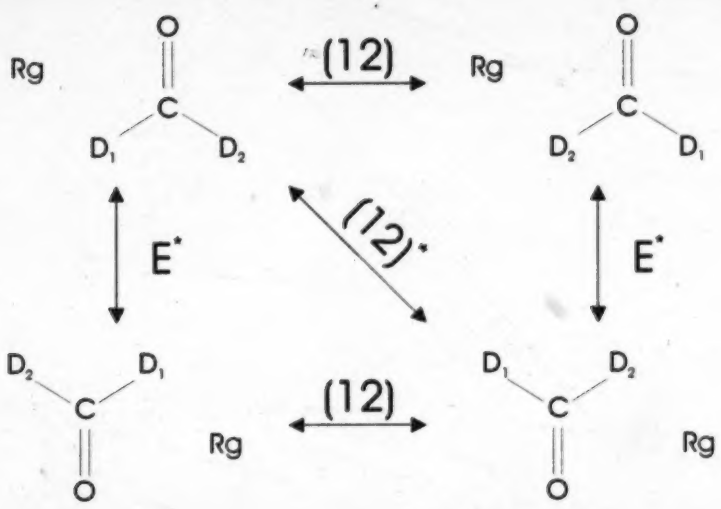

Figure 3.2: The molecular symmetry group operations for Rg-D_2CO van der Waals complexes. (12) refers to the interchange of D_1 and D_2. E^* refers to the complete inversion of all molecular coordinates through the centre of mass. $(12)^*$ refers to the interchange of D_1 and D_2 with an inversion of all molecular coordinates through the centre of mass.

rotational wave function belongs to the A_1 representation. For odd K_c, the rotational wave function changes sign under those operations, and it belongs to the A_2 representation.

The representation for the tunnelling wave function for Rg-D_2CO is the same as the representation for the tunnelling wave function for Rg-H_2CO. The tunnelling motion is involved with the operations (12) and $(12)^*$. As with Rg-H_2CO, the ground tunnelling state representation is A_1 and the first excited tunnelling state is B_2. The sign of the tunnelling wave function is unchanged under the A_1 representation.

The molecular symmetry representation for the nuclear spin wave function[34] (Γ_{spin}) changes. The spin of deuterium is 1. Three separate orientations are possible for each

deuterium nucleus, up (+1), even (0), and down (-1). To determine the nuclear spin wave function representation, the different permutations of nuclear spin orientation are tested under the symmetry group operations. Table 3.3 shows the different spin orientations and their value under each symmetry group operation. The nuclear spin wave function representation decomposes into $6A_1 \oplus 3B_2$. It is convenient to identify which spin states each representation belongs to. Each deuterium nucleus has spin 1 and with two deuterium atoms in D_2CO, the possible total spins are 2, 1 and 0. Spins 2 and 0 are associated with the A_1 nuclear spin wave function representation, while spin 1 is associated with B_2 nuclear spin wave function representation.

As with Rg-H_2CO, the symmetry representations of the various parts of the total wave function can be combined to give the right symmetry representation, A_1 or A_2, of the total wave function. The analysis of the ground tunnelling state is as follows:

$$\Gamma_{total} = \Gamma_{elec}\Gamma_{vib}\Gamma_{rot}\Gamma_{tun}\Gamma_{spin}$$

$$A_1 \otimes A_1 \otimes \begin{pmatrix} A_1 \\ A_2 \end{pmatrix} \otimes A_1 \otimes (6A_1 \oplus 3B_2) = \begin{pmatrix} 6A_1 \\ 6A_2 \end{pmatrix} \oplus \begin{pmatrix} 3B_2 \\ 3B_1 \end{pmatrix} \qquad (3.5)$$

In the tunnelling ground state, rotational wave functions with the even K_c, i.e. with A_1 symmetry, can only combined with nuclear spin functions of A_1 symmetry to give a A_1 symmetry for the total wave function. The spin weight of these rotational levels is six. Rotational wave functions with odd K_c (A_2 symmetry) can also combine with nuclear spin functions of A_1 symmetry to give total symmetry A_2.

A similar analysis for the first excited tunnelling state reveals the following:

Table 3.3: Spin Orientation under Symmetry Group Operations for Rg-D_2CO.

D_1	D_2	E	(12)	E^*	$(12)^*$
α	α	1	1	1	1
α	β	1	0	1	0
β	α	1	0	1	0
α	γ	1	0	1	0
γ	α	1	0	1	0
β	β	1	1	1	1
β	γ	1	0	1	0
γ	β	1	0	1	0
γ	γ	1	1	1	1
	Σ	9	3	9	3

α - spin up, β - spin even,
γ - spin down

$$\Gamma_{total} = \Gamma_{elec}\Gamma_{vib}\Gamma_{rot}\Gamma_{tun}\Gamma_{spin}$$

$$A_1 \otimes A_1 \otimes \begin{pmatrix} A_1 \\ A_2 \end{pmatrix} \otimes B_2 \otimes \left(6A_1 \oplus 3B_2\right) = \begin{pmatrix} 3A_1 \\ 3A_2 \end{pmatrix} \oplus \begin{pmatrix} 6B_2 \\ 6B_1 \end{pmatrix} \qquad (3.6)$$

Here, rotational wave functions with even (odd) K_c, i.e. A_1 (A_2) symmetry, can combine with B_2 nuclear spin functions to give A_1 (A_2) symmetry of the total wave function. The spin weight of levels in the excited tunnelling state is three. As for the Rg-H_2CO, the excited tunnelling state is metastable and its rotational spectra can be observed.

3.2.3 NUCLEAR QUADRUPOLE ANALYSIS

Another significant result comes from the analysis of Rg-D_2CO. The deuterium nucleus has spin 1 and possesses an electric quadrupole moment. In microwave

spectroscopy, the interaction of the nuclear quadrupole moment with the molecular electric field gradient splits the rotational energy levels, and leads to nuclear quadrupole hyperfine structure of rotational transitions. The nuclear spin state of a quadrupolar nucleus can be determined from an analysis of the hyperfine structure in a rotational spectrum. In the present study of Rg-D_2CO, the molecular symmetry group analysis found that nuclear spin wave function of A_1 symmetry is associated with total nuclear spin 2 and 0 and the nuclear spin wave function of B_2 symmetry is associated with total nuclear spin 1. Thus the ground tunnelling state will have hyperfine structure associated with nuclear spin 2 and 0 while the first excited tunnelling state will have hyperfine structure associated with nuclear spin 1. The distinct appearances of spectra in the two tunnelling states will therefore allow unambiguous assignment of the tunnelling state.

CHAPTER FOUR

Ar-D_2CO

4.1 INTRODUCTION

Formaldehyde can be considered the simplest organic compound containing a carbonyl group. As such, it can be used as a prototype to characterize the behaviour of the carbonyl group in weak intermolecular interactions. Consequently, a number of van der Waals complexes that contain the formaldehyde subunit has been investigated by high resolution spectroscopic methods. Rotational spectra of the following complexes were reported: HF-H_2CO,[36,37] HCl-H_2CO,[38,39] HCN-H_2CO,[40] HCCH-H_2CO,[41] H_2CO-H_2CO,[42] CO_2-H_2CO,[43] Ar-H_2CO,[10] H_2O-H_2CO,[44] and ClF-H_2CO.[45] Ar-H_2CO was studied by Novick,[10] using a Fourier Transform microwave spectrometer. Two tunnelling states were observed that are due to an exchange of the two equivalent hydrogen nuclei through an internal rotational motion of the formaldehyde subunit about its symmetry axis. Spectra of the protonated and fully deuterated forms were measured. For the protonated form, both a- and b-type transitions were measured. The assignments were confirmed by frequency loops and consistent spectroscopic fits. In addition, dipole moment components of μ_a = 0.461D and μ_b = 2.209D were determined for Ar-H_2CO from Stark shift measurements. For the deuterated form, a-type transitions were measured, but only one b-type transition was tentatively assigned. The assignment for Ar-D_2CO was left ambiguous and the purpose of the present work is to verify the assignment and to find further transitions. Furthermore, there was a possibility to measure the components of the deuterium nuclear quadrupole hyperfine structure that could not be resolved in the previous study. An

analysis of the nuclear quadrupole hyperfine structure would also help to confirm the assignment of the two tunnelling states involved.

4.2 EXPERIMENTAL

The experiments were performed using the Fourier Transform microwave spectrometer described in Chapter two. All transitions showing hyperfine structure were recorded at 120ns to increase the resolution of the spectra. The sample conditions used to characterize the van der Waals complex Ar-D_2CO spectroscopically were 4% Argon and 0.4% D_2CO with Neon as backing gas at a total pressure of 3.2 atm. The entire sample system was heated, along with the copper tubing leading from the sample containers to the pulsed nozzle, with heating tape to prevent the formaldehyde from condensing back into paraformaldehyde. Sufficient time was needed for the entire sample to reach a constant temperature and for the signal strength to become optimal, usually an hour. Samples were removed from the sample system at the end of every day to prevent the entire sample system from being coated with a thin film of paraformaldehyde that could interfere with the preparation of a new sample by increasing the amount of formaldehyde after heating the sample system.

4.3 SPECTRAL SEARCH AND ASSIGNMENT

From the Novick work[10] on Ar-H_2CO and Ar-D_2CO, the determined rotational and centrifugal distortion constants for Ar-D_2CO were used to predict the frequencies of the 1_{01}-0_{00} a-type transitions (one for each tunnelling state). The transitions were found at the

predicted frequencies thus confirming the assignment of the a-type transition of Ar-D_2CO by Novick.[10] All of Novick's transitions were re-measured to resolve the deuterium nuclear quadrupole hyperfine structure. The b-type transitions for Ar-D_2CO were not found in the Novick study and a spectral search was required. Confirmation of a potential b-type transition can be found by using a frequency loop since b-type transitions are between $K_a = 0$ and $K_a = 1$ energy levels. With a possible b-type transition, the frequency of another b-type transition can be calculated and immediately confirmed or discarded. In the present study, a spectral search for the 3_{13}-4_{04} b-type transition was done. The frequency region around the initially predicted frequency was searched. No transitions were found, and the spectral search region was lowered successively. When a candidate for the b-type transition was found, the corresponding frequency of the 4_{14}-5_{05} transition was calculated and checked for immediate confirmation. The 3_{13}-4_{04}/4_{14}-5_{05} pair of transitions was used for this search procedure since they both fall into the 8-18 GHz region. The electronic components of the spectrometer need not be changed, thus allowing easy checking of the 4_{14}-5_{05} transition. Once the two b-type transitions were found, the remaining b-type transitions in the spectrometer's frequency range were immediately measured. All measured transitions of both the ground tunnelling state and the first excited tunnelling state are shown in Tables 4.1 and 4.2 respectively, together with the quantum number assignments. The deuterium nuclear quadrupole hyperfine components are labelled using the coupling scheme, $\mathbf{F} = \mathbf{J} + \mathbf{I}$, where $\mathbf{I}$ is the total nuclear spin angular momentum $\mathbf{I} = \mathbf{I}_1 + \mathbf{I}_2$. $\mathbf{J}$ is the rotational angular momentum, and $\mathbf{F}$ is the resulting total angular momentum.

Table 4.1: Transitions of the Ground Tunnelling State of Ar-D_2CO.

J'Ka'Kc'-J"Ka"Kc" F'I'-F"I"	ν_{obs}[a] ν_{obs} (MHz)	$\Delta\nu$[b]	J'Ka'Kc'-J"Ka"Kc" F'I'-F"I"	ν_{obs}[a] ν_{obs} (MHz)	$\Delta\nu$[b]
101-000	4082.7199	-7.9	312-211	12449.0704	8.7
2 2-2 2	4082.7398	-0.5	4 2-4 2	12449.0793	0.9
1 0-0 0	4082.7398	2.1	3 2-3 2	12449.0793	0.0
3 2-2 2	4082.7130	-1.0	3 2-2 2	12449.0793	1.6
1 2-2 2	4082.6810	-0.6	4 2-3 2	12449.0740	0.3
			5 2-4 2	12449.0658	-1.9
111-202	22809.2248	-5.7	3 0-2 0	12449.0658	-1.0
1 2-0 2	22809.2585	-2.8	1 2-0 2	12449.0658	0.1
1 2-1 2	22809.2478	1.1			
3 2-4 2	22809.2346	0.3	313-212	12034.7803	5.5
3 2-3 2	22809.2075	-1.7	4 2-4 2	12034.8006	-2.0
2 2-3 2	22809.2052	1.0	3 2-3 2	12034.8006	4.8
2 2-2 2	22809.1976	2.1	3 2-2 2	12034.7897	1.0
			4 2-3 2	12034.7820	-0.3
202-101	8164.3513	-10.7	3 0-2 0	12034.7757	-2.5
1 2-1 2	8164.3744	-0.5	5 2-4 2	12034.7757	-1.0
3 2-3 2	8164.3744	0.6			
0 2-1 2	8164.3576	-2.7	313-404	14304.5749	8.3
2 2-2 2	8164.3576	1.3	5 2-6 2	14304.5746	-0.7
4 2-3 2	8164.3473	-1.4	4 2-5 2	14304.5746	-2.4
3 2-2 2	8164.3473	-0.2	3 0-4 0	14304.5746	1.5
1 2-2 2	8164.3167	0.5	3 2-4 2	14304.5746	-1.1
2 0-1 0	8164.3167	2.5	4 2-4 2	14304.5648	2.7
211-110	8300.6875	4.0	404-303	16319.9942	3.2
2 2-2 2	8300.7078	-1.1			
3 2-2 2	8300.7078	0.5	413-312	16595.0934	6.1
1 2-2 2	8300.6986	-2.7			
2 0-1 0	8300.6986	0.2	414-313	16043.0731	6.7
4 2-3 2	8300.6814	0.2	4 2-3 2	16043.0776	0.9
1 2-1 2	8300.6538	0.1	3 2-2 2	16043.0776	0.8
0 2-1 2	8300.6538	2.8	5 2-4 2	16043.0716	-1.4
			4 0-3 0	16043.0716	-0.8
212-111	8024.3636	-0.4	6 2-5 2	16043.0716	0.5
2 2-2 2	8024.3898	1.7			
3 2-2 2	8024.3811	0.1	414-505	9955.8112	0.3
3 2-3 2	8024.3766	0.6	5 2-6 2	9955.8166	2.5
4 2-3 2	8024.3573	1.6	4 2-5 2	9955.8166	1.5
1 2-1 2	8024.3406	-3.9	6 2-7 2	9955.8075	-2.7
			4 0-5 0	9955.8075	-0.9
212-303	18589.7841	1.3	3 2-4 2	9955.8075	-1.3
2 2-2 2	18589.8106	0.0	2 2-3 2	9955.8075	0.9
4 2-5 2	18589.7867	-0.4			
2 0-3 0	18589.7867	1.5	505-606	20391.8326	10.4
2 2-3 2	18589.7762	-1.1			
3 2-3 2	18589.7664	-3.8	514-413	20737.9704	-11.4
4 2-4 2	18589.7664	3.7			

Table 4.1 Continued.

J'Ka'Kc'-J"Ka"Kc" F'I'-F"I"	ν_{cal}[a] ν_{obs} (MHz)	$\Delta\nu$[b]	J'Ka'Kc'-J"Ka"Kc" F'I'-F"I"	ν_{cal}[a] ν_{obs} (MHz)	$\Delta\nu$[b]
			515-414	20048.5362	-6.6
303-202	12243.8011	-10.6			
4 2-4 2	12243.8275	3.4	515-606	5546.1110	4.1
3 2-3 2	12243.8086	-3.2	5 2-6 2	5546.1186	2.1
2 2-1 2	12243.8086	-1.3	6 2-7 2	5546.1186	4.4
1 2-0 2	12243.8086	1.7	7 2-8 2	5546.1066	-2.7
3 2-2 2	12243.8018	-1.3	4 2-5 2	5546.1066	-3.1
5 2-4 2	12243.8018	2.1	5 0-6 0	5546.1066	-1.1
4 2-3 2	12243.8018	2.8	3 2-4 2	5546.1066	0.3
2 2-2 2	12243.7656	-4.2			
			606-505	24458.2367	-2.0

[a]Calculated center line frequency.
[b]Observed-calculated frequencies in kHz from quadrupole fit.

Table 4.2: Transitions of the First Excited Tunnelling State of Ar-D_2CO.

J'Ka'Kc'-J"Ka"Kc" F'I'-F"I"	ν_{rot}[a] ν_{obs} (MHz)	$\Delta\nu$[b]	J'Ka'Kc'-J"Ka"Kc" F'I'-F"I"	ν_{rot}[a] ν_{obs} (MHz)	$\Delta\nu$[b]
101-000	4066.8817	-6.0	312-211	12371.4275	5.1
0 1-1 1	4066.9152	0.9	2 1-1 1	12371.4303	-0.1
2 1-1 1	4066.8850	0.0	4 1-3 1	12371.4303	1.3
1 1-1 1	4066.8645	-0.9	3 1-2 1	12371.4222	-1.2
111-202	22845.0089	-4.2	313-212	12019.0658	2.7
1 1-2 1	22845.0261	-1.0	4 1-3 1	12019.0686	0.7
2 1-2 1	22845.0261	1.2	2 1-1 1	12019.0686	2.4
2 1-3 1	22845.0030	-0.9	3 1-2 1	12019.0612	-0.5
0 1-1 1	22844.9894	0.6	3 1-3 1	12019.0406	-2.6
202-101	8132.8253	-8.5	313-404	14422.8633	5.0
1 1-1 1	8132.8591	1.1	2 1-3 1	14422.8710	4.7
3 1-2 1	8132.8261	-0.6	4 1-5 1	14422.8600	-3.5
2 1-1 1	8132.8261	0.8	3 1-4 1	14422.8600	-1.2
1 1-0 1	8132.8094	0.4			
2 1-2 1	8132.8040	-1.7	404-303	16258.1436	2.3
211-110	8248.8085	2.3	413-312	16491.9012	5.8
1 1-0 1	8248.8366	-2.6			
3 1-2 1	8248.8126	0.7	414-313	16022.3092	3.9
1 1-1 1	8248.7982	2.2			
2 1-1 1	8248.7920	-0.2	414-505	10129.5336	0.0
			3 1-4 1	10129.5360	-1.0
212-111	8013.8232	2.0	5 1-6 1	10129.5360	1.5
1 1-0 1	8013.8400	-1.4	4 1-5 1	10129.5294	-0.5
1 1-1 1	8013.8336	-2.1			
3 1-2 1	8013.8258	-1.9	505-404	20315.6364	6.3
2 1-2 1	8013.8108	0.6			
2 1-1 1	8013.8108	3.9	514-413	20609.5045	-8.5
212-303	18661.9384	1.8	515-414	20022.8822	-4.1
3 1-3 1	18661.9570	-1.9			
2 1-3 1	18661.9427	2.3	515-606	5783.9827	-2.6
1 1-2 1	18661.9427	3.0	4 1-5 1	5783.9857	-0.5
3 1-4 1	18661.9354	-1.7	6 1-7 1	5783.9857	1.5
2 1-2 1	18661.9092	-1.7	5 1-6 1	5783.9772	-1.1
303-202	12196.8916	-6.1	606-505	24368.4335	-1.0
2 1-2 1	12196.9217	0.7			
4 1-3 1	12196.8929	0.5			
3 1-2 1	12196.8929	1.3			
2 1-1 1	12196.8864	-2.0			
3 1-3 1	12196.8700	-0.6			

[a]Calculated center line frequency.
[b]Observed-calculated frequencies in kHz from quadrupole fit.

4.4 ANALYSIS, RESULTS AND DISCUSSION

The spectroscopic analysis of the observed transitions was done in a two step procedure. The deuterium nuclear quadrupole hyperfine structure was first analysed using the program Q4FIT. This program employs a first order perturbation treatment and fits nuclear quadrupole coupling constants χ_{aa}, χ_{bb} and the frequencies of the hypothetical unsplit rotational transitions to the observed splittings. The hypothetical centre line frequencies from the nuclear quadrupole hyperfine analysis were input for a fitting procedure to determine rotational and centrifugal distortion constants. Watson's A-reduction in its I^r representation was used.[46,47] The rotational constants A, B, C, the quartic centrifugal distortion constants Δ_J, Δ_{JK}, δ_J, and the sextic constant Φ_J were determined. The resulting rotational, centrifugal distortion, and nuclear quadrupole coupling constants are given in Table 4.3 for both ground and first excited tunnelling states.

4.4.1 IDENTIFICATION OF STATES

A main goal of the present study was to unambiguously establish the assignment of the two observed tunnelling states in the spectrum of Ar-D_2CO. From the molecular symmetry group analysis, the ground tunnelling state has total nuclear spin 2 and 0 associated with it, while the first excited tunnelling state has total nuclear spin 1 associated with it. Additionally, the intensity ratio of the ground tunnelling state to the first excited tunnelling state is predicted to be six to three, but due to the hyperfine structure associated with the rotational transitions, intensity is not a reliable indicator. The key feature for

Table 4.3: Determined Rotational, Distortion and Nuclear Quadrupole Coupling Constants for Ar-D_2CO.

Constants	Singlet	Triplet
A /MHz	33085.258(9)	33071.026(6)
B /MHz	2110.522(3)	2092.256(2)
C /MHz	1972.311(2)	1974.733(2)
Δ_J /kHz	26.36(6)	25.34(4)
Δ_{JK} /kHz	574.9(5)	463.4(3)
δ_J /kHz	1.59(3)	0.98(2)
Φ_J /Hz	2.1(9)	0.8(6)
χ_{aa} /kHz	58.40(92)	65.23(143)
χ_{bb} /kHz	-11.05(105)	-7.61(173)
S.D./kHz[a]	2.1	2.1
S.D./kHz[b]	8.7	5.9

[a] - standard deviation of the hyperfine fit.
[b] - standard deviation of the transition fit.

determining the identity of each state is how the quadrupole interaction splits a rotational transition into its hyperfine components. Intensity and spacing of the hyperfine components are used to identify the state.[48] For example, the 1_{01}-0_{00} transition of the ground tunnelling state (total nuclear spin I = 0,2) has four hyperfine components with an intensity ratio of 1 : 3.4 : 1 : 2.4 with a spacing between components of approximately 12 : 9 : 1. The spacing between the last two hyperfine components may be too small to resolve, but in this case, their intensities are additive giving three resolvable hyperfine components with an intensity ratio of 1 : 3.4 : 3.4 and with a spacing ratio of 1.3 : 1. The same transition in the first excited tunnelling state (total nuclear spin I = 1) has three hyperfine components with intensity ratio of 3 : 5 : 1 and a spacing ratio of 2 : 3. Thus, it is important to record the 1_{01}-0_{00} transition for both states to determine the identity of each state. Figure 4.1 shows the 1_{01}-0_{00} transition for both states of Ar-D_2CO with the

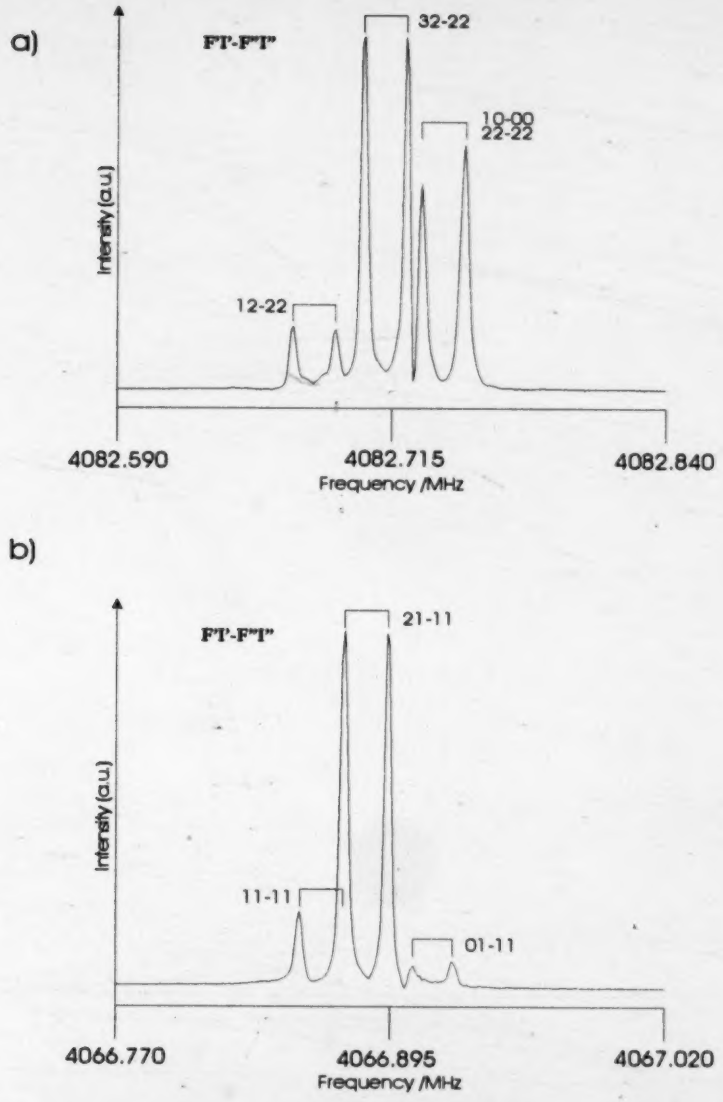

Figure 4.1: The $1_{01}-0_{00}$ transition of Ar-D_2CO in the ground tunnelling state and first excited tunnelling state are shown in (a) and (b), respectively. The hyperfine components are labelled with the F′I′−F″I″ notation where I is the total nuclear spin quantum number and F is the quantum number that describes the combined rotational and nuclear spin angular momentum. Each hyperfine component is seen as two lines due to Doppler splitting caused by the molecular beam being parallel to the axis of the microwave cavity.

individual hyperfine components labelled. Each hyperfine transition is split into two components due to the Doppler effect, and the transition frequencies are just the averages of the respective Doppler components. It is noted here that reliable intensity measurements are very difficult, if not impossible, to do with a Fourier Transform microwave spectrometer. One reason is that each hyperfine component has a different $\frac{\pi}{2}$ excitation pulse condition. However, in comparing Figures 4.1 a) and b), it is apparent that spectrum b) resembles much closer that of a spin 1 nucleus with intensity ratio 3:5:1, then spectrum a). Furthermore, the spacing of the components in spectrum b) is 1.5:1, in agreement with the ratio predicted for the first excited tunnelling state with total nuclear spin I = 1. The splitting ratio in spectrum a) is 1.2:1, close to the predicted ratio of 1.3:1 for the ground tunnelling state.

4.4.2 STRUCTURE DETERMINATION

From the determined rotational constants, A, B and C, effective structures can be derived for both ground and first excited tunnelling states. In this procedure, it is assumed that the known structure of H_2CO[6,7,8,9] remains unchanged upon complex formation with Ar. Three structural parameters remain to be determined. These can be, for example, R, the distance between the Ar atom and the centre of mass of the formaldehyde monomer, θ, the angle between the this distance and the C_2 axis of formaldehyde, and the dihedral angle, Φ, which describes the angle between the heavy atom plane and the plane of the formaldehyde monomer. There is insufficient information to determine the dihedral angle Φ, and it was set to zero in the fitting routine. Isotopic shrinkage was taken into account

for the deuterated species. Values of R = 3.632Å and θ = 80° were determined for the ground tunnelling state and R = 3.646Å and θ = 80° for the first excited tunnelling state. Figure 4.2 shows the determined structures for both the ground and first excited tunnelling states.

An *ab initio* study of Ar-H_2CO[49] that models the potential energy surface of this van der Waals complex was done previously. The global minimum for this complex corresponds to a planar geometry with the argon at a distance of 3.75Å from the centre of mass of the formaldehyde monomer. The angle defined by the formaldehyde's oxygen, centre of mass of the formaldehyde monomer and the argon atom is 80°. The experimental angle of 79.9° is surprisingly close to the *ab initio* value of 80° given the fact that calculations were done only every 20° in the Ar-H_2CO complex. The discrepancy in the calculated distance from the experimental distance is easy to account for as distances every 0.25Å were calculated.

4.4.3 NUCLEAR QUADRUPOLE COUPLING

The experimental deuterium nuclear quadrupole coupling constants in Table 4.4 may be compared with those based on the known monomer coupling constant[50] and the structure of the complex derived above. The principal coupling constant of D_2CO is 171 kHz[50] and this component is along the C-D bond. In order to find the nuclear quadrupole coupling constants of Ar-D_2CO, the projections of the monomer constant along the C-D bond onto the principal inertial axes of Ar-D_2CO need to be evaluated. The projections are given by equation 4.1:

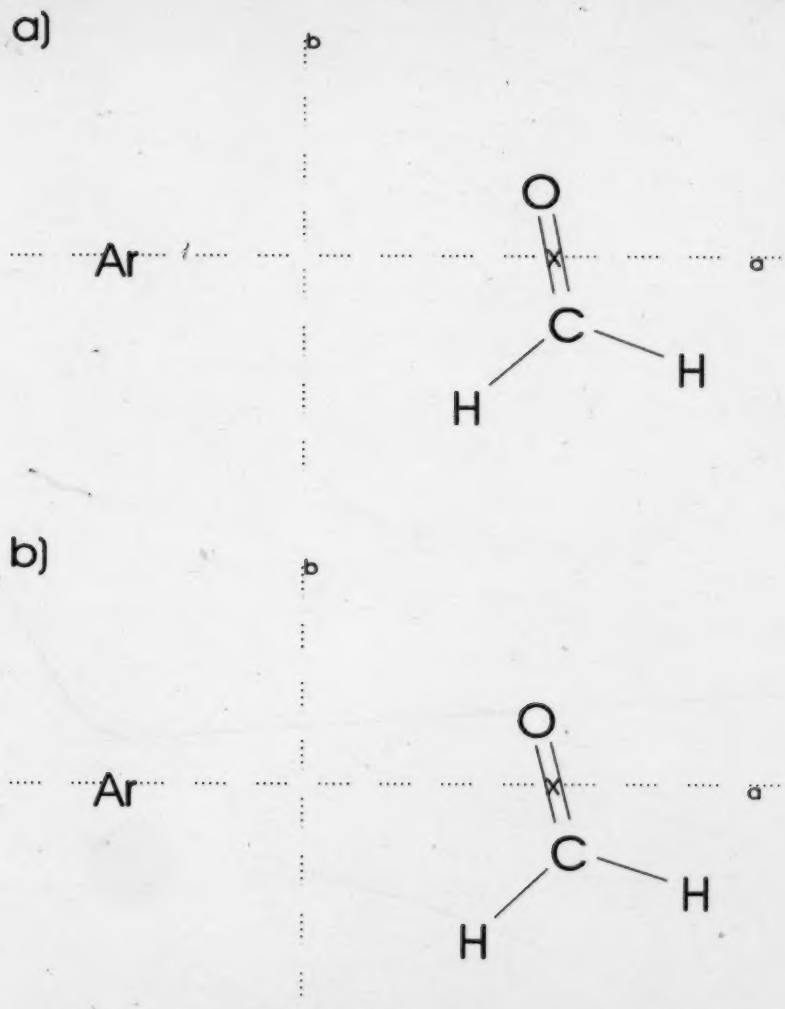

Figure 4.2 The Ar-H_2CO complex in its principal inertial axis system. The small (x) in the middle of the C-O bond represents the centre of mass of the formaldehyde monomer. The top figure (a) shows the effective structure of the ground tunnelling state. The distance from the argon atom to the centre of mass of the formaldehyde monomer is 3.632Å and the angle formed by the argon atom, formaldehyde's centre of mass and the oxygen atom is 80°. The bottom figure (b) shows the effective structure of the first excited tunnelling state. The distance from the argon atom to the centre of mass of the formaldehyde monomer is 3.646Å and the angle formed by the argon atom, formaldehyde's centre of mass and the oxygen atom is 80°.

Table 4.4: Calculated and Experimental Deuterium Nuclear Quadrupole Coupling Constants for Ar-D_2CO.

	Ground		First Excited	
	χ_{aa} (kHz)	χ_{bb} (kHz)	χ_{aa} (kHz)	χ_{bb} (kHz)
D_1	141.23	-55.73	142.28	-56.78
D_2	49.10	36.40	47.45	38.05
Average	95.16	-9.66	94.86	-9.36
Experimental	58.40	-11.05	65.23	-7.61

$$\chi_{mm} = \chi_0 \left\langle P_2(\cos\theta_m) \right\rangle;\ m = a,b,c \qquad (4.1)$$

Here, χ_0 is the monomer coupling constant, and θ_m is the angle between the C-D bond and the m-principal inertial axis. The brackets $\langle\rangle$ indicate averaging over the large amplitude motions.

Ar-D_2CO has two deuterium nuclei, so each deuterium atom contributes to the observed nuclear quadrupole coupling constant. For a given axis, the average of the two nuclear coupling constants is taken. The two deuterium atoms in the ground tunnelling state have angles with the a-axis of 19.9° and 43.6°, the deuterium atoms of the first excited tunnelling state have angles with the a-axis of 19.5° and 44.0°. The angles formed with the b-axis are just 90° less the angles formed with the a-axis. Shown in Table 4.4 are the calculated nuclear quadrupole coupling constants for the ground tunnelling state and the first excited tunnelling state. For comparison, the experimental constants are included as well as the individual constants for each deuterium nucleus along with the average nuclear quadrupole coupling constant.

The sum of χ_{aa}, χ_{bb} and χ_{cc} is zero and knowing the experimental values of χ_{aa} and

χ_{bb}, χ_{cc} is -47.35 kHz and -57.62 kHz for the ground tunnelling state and first excited tunnelling state, respectively. The calculated χ_{bb} coupling constants agree surprisingly well with the experimental ones, whereas the agreement for the χ_{aa} and χ_{cc} constants is much worse.

This confirms very nicely the current picture of the Ar-H_2CO complex, in which the formaldehyde subunit undergoes a hindered internal rotation about its C_2 symmetry axis. Since the C_2 axis of formaldehyde is nearly parallel to the b-axis of the complex, this internal motion does not affect the χ_{bb} values. χ_{aa} and χ_{cc}, however, are averages over this motion, and deviate from the calculated rigid structure values. In particular, if this complex were rigid, χ_{cc} of the complex would equal the χ_{cc} value of the monomer of -85.5 kHz. The experimental χ_{cc} values correspond to average angles of 67.3° and 70.8° between the c-axis of the complex and monomer for ground and first excited tunnelling states, respectively. These values were evaluated using equation 4.1. The corresponding average dihedral angles are 22.7° and 19.2° for ground and first excited tunnelling states, respectively.

4.5 CONCLUSIONS

The two tunnelling states of the Ar-D_2CO van der Waals complex have been properly identified by analysing the deuterium nuclear quadrupole hyperfine structure. The *ab initio* structure agrees with the derived structure, as do the χ_{bb} deuterium nuclear quadrupole coupling constants. The values for the χ_{aa} and χ_{cc} coupling constants confirm that the tunnelling motion is an internal rotation of the formaldehyde subunit about its C_2 axis.

CHAPTER FIVE

ROTATIONAL SPECTRA OF THE Ne-H_2CO AND Ne-D_2CO COMPLEXES

5.1 INTRODUCTION

High resolution spectroscopy of weakly bound complexes has delivered, and continues to deliver, some of the most accurate data that can be related to the corresponding interaction potential energy surfaces. A significant number of complexes that contain the formaldehyde subunit (HF-H_2CO,[36,37] HCl-H_2CO,[38,39] HCN-H_2CO,[40] HCCH-H_2CO,[41] H_2CO-H_2CO,[42] CO_2-H_2CO,[43] Ar-H_2CO,[10] H_2O-H_2CO,[44] and ClF-H_2CO[45]) has been studied in the past mainly for two reasons. Formaldehyde can be viewed as the simplest organic compound containing a carbonyl group, and its complexes can be considered as prototypes for weak interactions involving carbonyl groups. Secondly, formaldehyde has two equivalent hydrogen nuclei that can exchange places in the complex through an internal tunnelling motion. The complicated tunnelling dynamics can be deduced from the resulting effects on the rotational spectra, as, for example, outlined in Chapter three in this thesis.

Of the rare gas - formaldehyde complexes, only the argon containing variety was studied previously by Novick.[10] Subsequently, a more detailed study of the fully deuterated isotopomer was done, as described in Chapter four of this thesis. It was possible, in particular, to find unambiguous assignments of the two observed tunnelling states, based on the deuterium nuclear quadrupole hyperfine structure. An extension of the previous studies to the neon containing species is of interest for several reasons. It is anticipated that the weaker interaction with the less polarizable neon atom will result in a

lower barrier to the internal rotation tunnelling motion. In the rotational spectrum this would result in an increase of the tunnelling splitting as compared to Ar-H_2CO. Furthermore, neon occurs naturally as two isotopes with significant abundances (^{20}Ne, 90.5%, ^{22}Ne, 9.2%). The additional observable spectrum of the ^{22}Ne containing isotopomer would yield an additional set of spectroscopic parameters that can be used to further refine structural and dynamical information about the complex. Lastly, the smaller number of electrons in the neon atom as compared to the argon atom makes the Ne-H_2CO complex more amerable to high level electronic structure calculations. Indeed, an *ab initio* calculation of the Ne-H_2CO complex was performed, and is described in Chapter six of this thesis.

5.2 EXPERIMENTAL

The spectra were measured with the Fourier Transform microwave spectrometer described in Chapter two. All transitions showing hyperfine structure were recorded with 120ns sampling interval to increase the resolution of the spectra. The sample conditions used to measure the spectra of Ne-H_2CO and Ne-D_2CO van der Waals complexes were 0.4% H_2CO (D_2CO) with neon as backing gas at a total pressure of 3.2 atm. The entire sample system was heated, along with the copper tubing from the sample containers to the pulsed nozzle, with heating tape to prevent the formaldehyde from condensing back into paraformaldehyde. Sufficient time was needed for the entire sample to reach a constant temperature for the signal strength to become optimal, usually an hour.

5.3 SPECTRAL SEARCH AND ASSIGNMENT

An initial structure of the Ne-H_2CO complex was predicted, using the known structure of Ar-H_2CO as a starting point. All structural parameters remained unchanged, with the exception of the bond length R between the neon atom and the centre of mass of the formaldehyde subunit. The distance R was estimated to be 3.56Å in Ne-H_2CO, from a comparison with other Ne-, Ar- molecule pairs of van der Waals complexes (Ne-,[51] Ar-CO;[52] Ne-,[53] Ar-CO_2;[54,55] Ne-,[56,57] Ar-OCS[58,56]). The resulting structure is shown in Figure 5.1. Ne-H_2CO is a prolate asymmetric rotor, and both a- and b-type transitions are expected to occur.

The spectral search was started for the 2_{02}-1_{01} transition of ^{20}Ne-H_2CO. A strong line was found close to the predicted frequency. Its assignment was confirmed by finding the other lower and higher J transitions of the $K_a = 0$ stack, and the corresponding transition of the ^{22}Ne-H_2CO isotopomer. The frequencies of the $K_a = 0$ transitions are compiled in Table 5.1 for both ^{20}Ne-H_2CO and ^{22}Ne-H_2CO. Search and assignment of $K_a = 1$ transitions was very difficult due to a very large number of unassigned transitions found during the course of the spectral searches. Frequencies of two sets of possible $K_a = 1$ transitions, for ^{20}Ne-H_2CO and ^{22}Ne-H_2CO, respectively, are given in Table 5.2 together with a tentative quantum number assignment.

It was expected to find two sets of transitions that occur within different tunnelling states, similar to the situation in Ar-H_2CO.[10] However, despite extensive searches, no other set of transitions could be identified. It was hoped to resolve the mystery of the missing tunnelling state through an investigation of the neon complex with perdeuterated

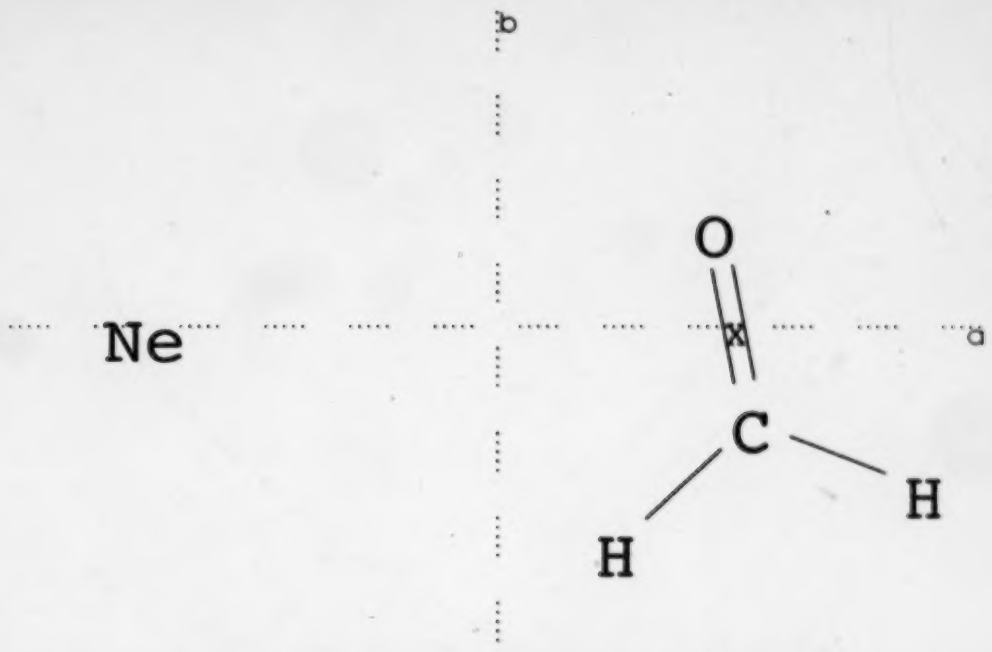

Figure 5.1: The Ne-H_2CO complex in its principal inertial axis system. The small (x) near the centre of the C-O bond represents the centre of mass of the formaldehyde monomer. The guess structure for Ne-H_2CO used to calculate the transitions of the complex. The distance from the neon atom to the centre of mass of the formaldehyde monomer is 3.56Å and the angle formed by the neon atom, formaldehyde's centre of mass and the oxygen atom is 80°. Both a- and b-type transitions are expected.

Table 5.1: Measured Ground Tunnelling State Frequencies for Ne-H_2CO.

$J'_{K_a'K_c'} - J''_{K_a''K_c''}$	^{20}Ne-H_2CO (MHz)	$\Delta\nu^a$ (kHz)	^{22}Ne-H_2CO (MHz)	$\Delta\nu^a$ (kHz)
$1_{01} - 0_{00}$	6515.2761	0.2	6184.4159	0.3
$2_{02} - 1_{01}$	13022.4887	-0.2	12361.754	-0.3
$3_{03} - 2_{02}$	19513.532	0.1	18524.9011	0.1
$4_{04} - 3_{03}$	25980.2100	0.0	24666.6667	0

[a]Observed-calculated frequencies in kHz.

Table 5.2: $K_a = 0$ and Possible $K_a = 1$ Transitions for Ne-H_2CO in MHz.

	^{20}Ne-H_2CO		^{22}Ne-H_2CO	
		$\Delta\nu^a$		$\Delta\nu^a$
$1_{01}-0_{00}$	6515.2761	0.2	6184.4159	0.3
$2_{02}-1_{01}$	13022.4887	-0.2	12361.7539	-0.3
$3_{03}-2_{02}$	19513.5320	0.1	18524.9011	0.1
$4_{04}-3_{03}$	25980.2100	0.0	24666.6667	0.0
$2_{12}-1_{11}$	12727.5743	0.0	12105.0707	0.0
$2_{11}-1_{10}$	13261.3872	0.0	12592.3721	0.0
$3_{13}-2_{12}$	19074.8240	0.0	18142.7998	0.0
$3_{12}-2_{11}$	19873.3744	0.0	18871.7313	0.0

[a]Observed-calculated frequencies in kHz.

formaldehyde. The larger mass of the deuterium nuclei would lead to a lower tunnelling probability and to a smaller frequency shift between the transitions within the two tunnelling states. A partially determined structure of Ne-H_2CO was used to predict a spectrum of Ne-D_2CO to start the spectral search. In determining a guess structure for Ne-D_2CO, the isotopic shrinkage of deuterated formaldehyde was taken into account. As with Ne-H_2CO, a parallel set of transitions was expected due to the other isotopomer of neon. Similar problems were encountered with Ne-D_2CO as with Ne-H_2CO, the $K_a = 0$ transitions were positively identified. The deuterium nuclear quadrupole hyperfine structure could be partially resolved. Figure 5.2 shows two sample transitions. Table 5.3 shows the frequencies of the $K_a = 0$ transitions for ^{20}Ne-H_2CO and ^{22}Ne-H_2CO in the ground tunnelling state labelled with the quantum number assignments. The deuterium

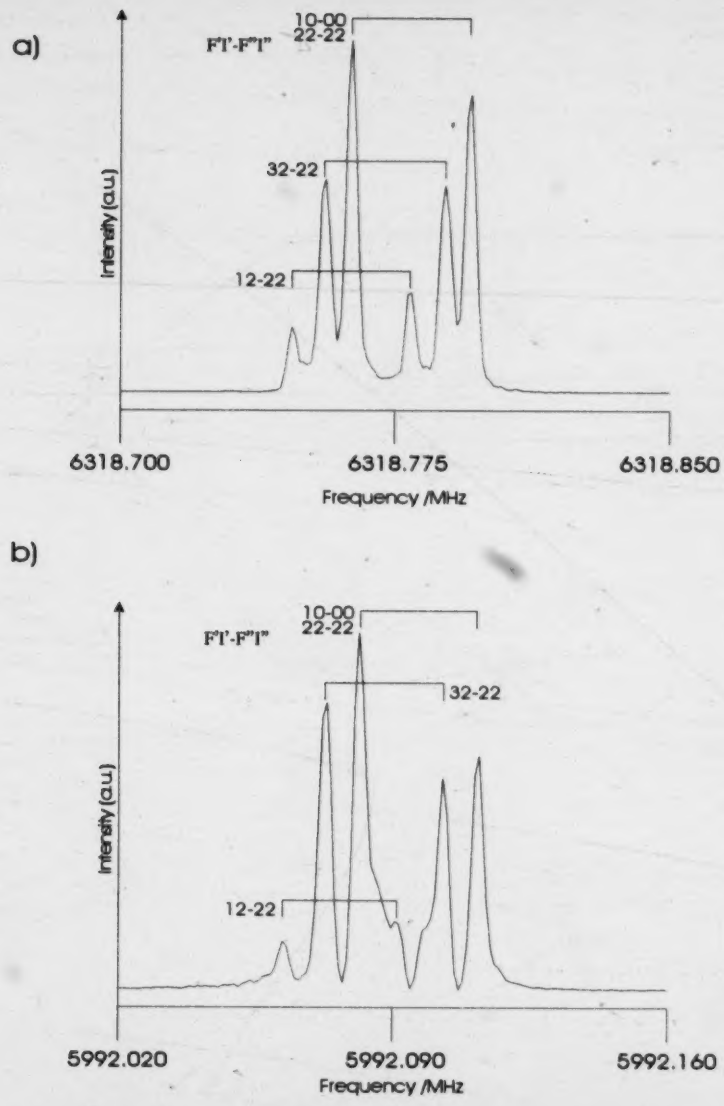

Figure 5.2 The 1_{01}-0_{00} transitions of Ne-D_2CO in the ground tunnelling state for ^{20}Ne-D_2CO and ^{22}Ne-D_2CO are shown in (a) and (b), respectively. The hyperfine components are labelled with the F′I′−F″I″ notation where I is the total nuclear spin quantum number and F is quantum number that describes the combined rotational and nuclear spin angular momentum. Each hyperfine component is seen as two lines due to Doppler splitting caused by the molecular beam being parallel to the axis of the microwave cavity.

Table 5.3: $K_a = 0$ Transitions of the Ground Tunnelling State of Ne-D_2CO.

	^{20}Ne-D_2CO		^{22}Ne-D_2CO	
J'Ka'Kc'-J"Ka"Kc" F'I'-F"I"	ν_{cf}[a] ν_{obs} (MHz)	$\Delta\nu$[b]	ν_{cf}[a] ν_{obs} (MHz)	$\Delta\nu$[b]
101-000	6318.7750	0.1	5992.0907	0.0
2 2-2 2	6318.7804	-1.0	5992.0974	-0.3
1 0-0 0	6318.7804	-0.2	5992.0974	0.6
3 2-2 2	6318.7732	0.1	5992.0887	0.0
1 2-2 2	6318.7641	1.1	5992.0772	-0.3
202-101	12628.9523	-0.1	11976.7807	0.0
1 2-1 2	12628.9600	0.1	11976.7884	-0.6
3 2-3 2	12628.9600	0.9	11976.7884	0.2
4 2-3 2	12628.9514	-0.2	11976.7797	-0.2
3 2-2 2	12628.9514	0.5	11976.7797	0.5
1 2-2 2	12628.9405	-0.9	11976.7685	-0.3
2 0-1 0	12628.9405	-0.4	11976.7685	0.4
303-202	18921.9247	0.0	17946.6581	0.0
404-303	25189.0633	0.0	23894.2898	0.0

[a]Centre line frequency from hyperfine fit.
[b]Observed-calculated frequencies in kHz.

nuclear quadrupole hyperfine components are labelled using the coupling scheme, $\mathbf{F} = \mathbf{J} + \mathbf{I}$, where $\mathbf{I}$ is the total nuclear spin angular momentum $\mathbf{I} = \mathbf{I}_1 + \mathbf{I}_2$. $\mathbf{J}$ is the rotational angular momentum, and $\mathbf{F}$ is the resulting total angular momentum. As with the Ne-H_2CO isotopomers, only a tentative assignment for the transitions with $K_a = 1$ could be achieved. Often, nuclear quadrupole hyperfine structure of rotational transitions can be used to unambiguously assign the rotational quantum numbers. In the present case, however, the hyperfine structures were only of limited value in the assignment procedure because of the very narrow splittings. The frequencies of tentatively assigned $K_a = 1$ transitions of ^{20}Ne-H_2CO and ^{22}Ne-H_2CO are given in Table 5.4.

Table 5.4: Transitions of the Ground Tunnelling State of Ne-D_2CO.

	^{20}Ne-D_2CO		^{22}Ne-D_2CO	
J'Ka'Kc'-J"Ka"Kc" F'I'-F"I"	ν_{rot}[a] ν_{obs} (MHz)	$\Delta\nu$[b]	ν_{rot}[a] ν_{obs} (MHz)	$\Delta\nu$[b]
101-000	6318.7750	137.2	5992.0907	-171.5
2 2-2 2	6318.7804	-1.0	5992.0974	-0.4
1 0-0 0	6318.7804	-0.2	5992.0974	0.5
3 2-2 2	6318.7732	0.0	5992.0887	0.1
1 2-2 2	6318.7641	1.1	5992.0772	-0.1
202-101	12628.9523	73.7	11976.7807	-78.9
1 2-1 2	12628.9600	0.3	11976.7884	-0.6
3 2-3 2	12628.9600	0.6	11976.7884	-0.2
4 2-3 2	12628.9514	-0.1	11976.7797	-0.2
3 2-2 2	12628.9514	0.2	11976.7797	0.3
1 2-2 2	12628.9405	-0.8	11976.7685	0.0
2 0-1 0	12628.9405	-0.2	11976.7685	0.7
211-110	12819.5978	-105.7	12166.2609	125.5
3 2-2 2	12819.6022	-2.6	12166.2681	0.4
2 2-2 2	12819.6022	-1.6	12166.2681	-0.4
4 2-3 2	12819.5946	-1.8	12166.2586	0.0
3 2-3 2	12819.5946	1.0	12166.2586	-2.3
0 2-1 2	12819.5866	1.6	12166.2502	1.8
1 2-1 2	12819.5866	3.3	12166.2502	0.5
212-111	12319.3903	-105.2	11691.6164	124.9
3 2-2 2	12319.3974	2.4	11691.6244	1.8
3 2-3 2	12319.3974	-0.6	11691.6244	4.1
4 2-3 2	12319.3876	0.3	11691.6114	-2.4
1 2-1 2	12319.3876	-0.7	11691.6056	-3.6
0 2-1 2	12319.3806	-1.5	11691.6056	0.1
303-202	18921.9247	-182.3	17946.6581	212.6
312-211	19209.2088	119.4	18234.7084	-141.8
313-212	18467.5839	121.7	17500.1470	-144.3
4 2-4 2	18467.5964	1.5	17500.1552	0.8
3 2-3 2	18467.5964	5.8	17500.1552	2.8
3 2-2 2	18467.5832	-3.7	17500.1461	-4.0
4 2-3 2	18467.5832	-1.0	17500.1461	-1.8
3 0-2 0	18467.5832	-0.5	17500.1461	-0.3
5 2-4 2	18467.5832	0.6	17500.1461	0.1
2 2-2 2	18467.5674	-2.4	17500.1410	2.4
404-303	25189.0633	65.6	23894.2898	-77.2
413-312	25579.8090	-36.7	24285.4158	43.6

Table 5.4 (continued).

	^{20}Ne-D_2CO		^{22}Ne-D_2CO	
J'Ka'Kc'-J"Ka"Kc" F'I'-F"I"	ν_{rot}[a] ν_{obs} (MHz)	$\Delta\nu$[b]	ν_{rot}[a] ν_{obs} (MHz)	$\Delta\nu$[b]
414-313	24593.5979	-38.6	23268.7983	45.9

[a]Center line frequency from hyperfine fit.

[b]Observed-calculated frequencies in kHz.

5.4 ANALYSIS, RESULTS AND DISCUSSION

Since the assignment of the transitions with $K_a = 1$ is only tentative, two different analyses were carried out. One included only $K_a = 0$ transitions that were fit with a pseudodiatomic model to obtain the rotational constant (B +C)/2, quartic centrifugal distortion constant Δ_J and sextic centrifugal distortion constant Φ_J. Table 5.5 contains the results for ^{20}Ne-H_2CO and ^{22}Ne-H_2CO. The second analysis included all transitions and employed Watson's A-reduction semi-rigid rotor Hamiltonian in its I^r representation.[46,47] The rotational constants B and C, the quartic centrifugal distortion constants Δ_J, Δ_{JK}, δ_J and the sextic centrifugal distortion constants Φ_J and Φ_{JK} were fit to the measured transitions frequencies. The value of the A rotational constant was fixed at 39.780 GHz, obtained from the initial guess structure of Ne-H_2CO. The values of all other centrifugal distortion constants were fixed at zero in the fitting procedure. The results are given in Table 5.6 for ^{20}Ne-H_2CO and ^{22}Ne-H_2CO.

The analysis of the Ne-D_2CO transitions with deuterium nuclear quadrupole hyperfine structure preceded the rotational and centrifugal distortion analysis. The deuterium nuclear quadrupole hyperfine structure was treated as a first order perturbation. The fitting procedure yielded the nuclear quadrupole coupling constants χ_{aa} and χ_{bb} along with the frequencies of the hypothetical unsplit rotational transitions. The hypothetical unsplit centre line rotational frequencies were used in the fit of the rotational and centrifugal distortion constants. Table 5.7 contains the rotational and centrifugal distortion constants from the fit of the $K_a = 0$ transitions of ^{20}Ne-D_2CO and ^{22}Ne-D_2CO. Table 5.8 shows the rotational, centrifugal distortion and deuterium nuclear quadrupole

Table 5.5: Determined Constants for Ne-H_2CO.

Constants		^{20}Ne-H_2CO	^{22}Ne-H_2CO
(B+C)/2	/MHz	3258.2761(1)	3092.7638(2)
Δ_J	/kHz	318.94(1)	277.87(2)
Φ_J	/Hz	-61.2(4)	-52.0(6)
S.D.	/kHz	0.3	0.4

Table 5.6: Determined Constants for Ne-H_2CO.

Constant		^{20}Ne-H_2CO	^{22}Ne-H_2CO
B	/MHz	3391.9284(2)	3214.7896(3)
C	/MHz	3124.4449(2)	2970.6011(3)
Δ_J	/kHz	274.20(2)	243.63(2)
Δ_{JK}	/MHz	7.3477(1)	3.5153(2)
δ_J	/kHz	18.033(6)	16.807(8)
Φ_J	/Hz	-82.5(5)	-75.3(6)
Φ_{JK}	/kHz	-2.608(9)	-5.85(1)
S.D.	/kHz	0.3	0.4

coupling constants for ^{20}Ne-D_2CO and the ^{22}Ne-D_2CO from the simultaneous fit of $K_a \neq 0$ and 1 transitions.

5.4.1 IDENTIFICATION OF THE STATE

The initial investigation into the Ne-H_2CO complexes centred on the non-deuterated formaldehyde species. After only one state was found, the question arose as to

Table 5.7: Determined Constants for Ne-D_2CO.

Constants		^{20}Ne-D_2CO	^{22}Ne-D_2CO
(B+C)/2	/MHz	3160.0770(1)	2996.6351(1)
Δ_J	/kHz	344.756(7)	294.818(3)
Φ_J	/Hz	-14.4(2)	-15.09(9)
χ_{aa}	/kHz	18.4(6)	20.1(4)
S.D.	/kHz[a]	0.8	0.5
S.D.	/kHz[b]	0.1	0.1

[a] - standard deviation of the hyperfine fit.
[b] - standard deviation of the rotational fit.

Table 5.8: Determined Rotational, Distortion and Deuterium Nuclear Quadrupole Coupling Constants for Ne-D_2CO.

Constants		^{20}Ne-D_2CO	^{22}Ne-D_2CO
B	/MHz	3286.8(2)	3112.0(3)
C	/MHz	3032.9(2)	2881.3(3)
Δ_J	/kHz	280.4(87)	268.3(104)
Δ_{JK}	/MHz	15.51(7)	11.07(9)
δ_J	/kHz	139.(12)	-213.(15)
Φ_J	/kHz	-0.4(3)	0.8(3)
Φ_{JK}	/kHz	36.(29)	-161.(3)
Φ_1	/kHz	3.4(4)	-1.2(4)
χ_{aa}	/kHz	18.3(12)	20.4(11)
χ_{bb}	/kHz	6.6(25)	-5.3(23)
S.D.	/kHz[a]	2.2	2
S.D.	/kHz[b]	240.8	285.5

[a] - standard deviation of the hyperfine fit.
[b] - standard deviation of the rotational fit.

which state had been found. To help identify the observed tunnelling state of Ne-H_2CO, the corresponding complex using deuterated formaldehyde Ne-D_2CO was studied. The transitions of the Ne-D_2CO complex were expected to show deuterium nuclear quadrupole coupling hyperfine structure. From the molecular symmetry group analysis (see Chapter three), different total nuclear spins are associated with each tunnelling state: total nuclear spin I = 0 and 2 with the ground tunnelling state and total nuclear spin I =1 with the first excited tunnelling state. The intensity and spacing of the hyperfine components can then be used to identify the state observed. The appearance of the deuterium nuclear quadrupole hyperfine structure is expected to be similar to that of Ar-D_2CO since the structures of the complexes are expected to be similar. The $J_{KaKc} = 1_{01}$-0_{00} transition is the most informative transition in determining the identity of the tunnelling states. For this transition, the ground tunnelling state has four hyperfine components. However, with Ar-D_2CO, two of the hyperfine components were too close to be resolved and their intensities were additive. It was expected that Ne-D_2CO would follow this pattern with three resolvable hyperfine components. Their intensity ratio was predicted to be 1:3.4:3.4 with a spacing ratio of 1.3:1. The first excited tunnelling state (total nuclear spin I = 1) was predicted to have three hyperfine components with an intensity ratio of 3:5:1 and a spacing ratio of 2:3 for the $J_{KaKc} = 1_{01}$-0_{00} transition. Figure 5.2 shows the $J_{KaKc} = 1_{01}$-0_{00} transition for both ^{20}Ne-D_2CO and ^{22}Ne-D_2CO in the only state observed. Each hyperfine transition is split into two components due to the Doppler effect. Reliable intensity measurements are difficult to obtain with Fourier Transform microwave spectroscopy due to each hyperfine component having a different $\frac{\pi}{2}$ excitation pulse condition. However,

the intensity patterns of the spectra in figure 5.2 resemble those predicted for the ground tunnelling state. In addition, the frequency spacing is in the ratio 1.3:1, in agreement with the predicted ratio for the ground tunnelling state.

5.4.2 STRUCTURE DETERMINATION

A structure was determined for Ne-H_2CO using only the (B + C)/2 rotational constants obtained from the confirmed $K_a = 0$ transitions of Ne-H_2CO and Ne-D_2CO for the ground tunnelling state. It is assumed that the known structure of H_2CO[6,7,8,9] remains unchanged upon complex formation with neon. Three structural parameters remained to be determined. These parameters are, R, the distance from the neon atom to the centre of mass of the formaldehyde monomer, θ, the angle between the R distance and the C_2 axis of formaldehyde, and Φ, the dihedral angle between the heavy atom plane and the formaldehyde monomer plane. The dihedral angle could not be determined as not enough information was available and was set to zero in the fitting procedure. Isotopic shrinkage was taken into account for the deuterated species. Values of R = 3.492Å and $\theta = 108°$ were determined for the ground tunnelling state of Ne-H_2CO. Figure 5.3 shows the determined structure for Ne-H_2CO in the ground tunnelling state.

An *ab initio* study of Ne-H_2CO, described in chapter six, models the potential energy surface of this van der Waals complex. The global minimum for this complex was found to have a planar geometry with the neon at a distance of 3.50Å from the centre of mass of the formaldehyde monomer. The neon atom is located at an angle of 80° formed by the formaldehyde's oxygen, the centre of mass of the formaldehyde monomer and the

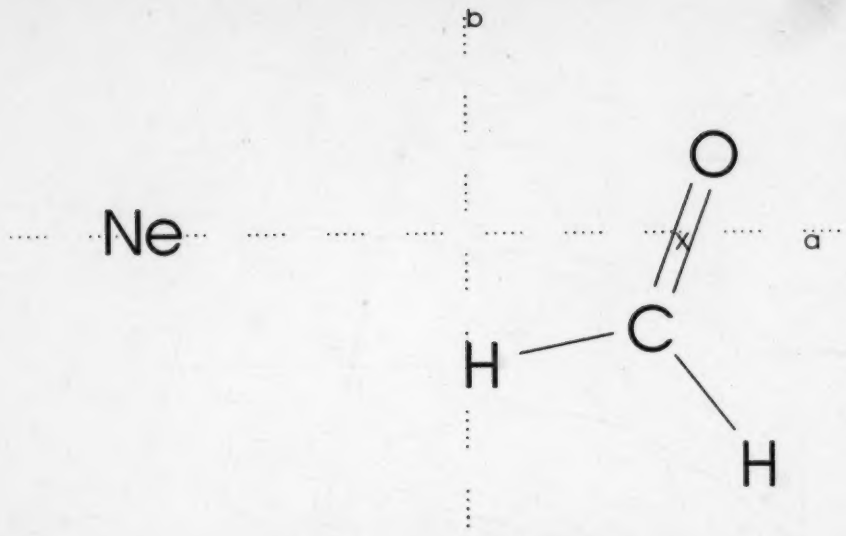

Figure 5.3 The Ne-H_2CO complex in its principal inertial axis system. The small (x) near the centre of the C-O bond represents the centre of mass of the formaldehyde monomer. The ground tunnelling state effective structure is shown above. The distance from the neon atom to the centre of mass of the formaldehyde monomer is 3.492Å and the angle formed by the neon atom, formaldehyde's centre of mass and the oxygen atom is 108°.

neon atom. The experimental values of R = 3.492Å is very close to the *ab initio* value of R = 3.50Å (see Chapter six). The discrepancy between the experimental angle (θ = 108°) and the *ab initio* angle (θ = 80°) may be due to the fact that the rotational constant was determined using only the $K_a = 0$.

5.4.3 NUCLEAR QUADRUPOLE COUPLING

The deuterium nuclear quadrupole coupling constants obtained from the fit of the observed hyperfine pattern can be used to deduce additional information about the structure and the internal dynamics of Ne-H_2CO. The experimental deuterium nuclear

Table 5.9: Calculated and Experimental Deuterium Nuclear Quadrupole Coupling Constants for Ne-D_2CO in the Ground Tunnelling State.

	^{20}Ne-D_2CO			^{22}Ne-D_2CO		
	χ_{aa} (kHz)	χ_{bb} (kHz)	χ_{cc} (kHz)	χ_{aa} (kHz)	χ_{bb} (kHz)	χ_{cc} (kHz)
D_1	158.2	-72.7	-85.5	158.03	-72.53	-85.5
D_2	17.89	67.61	-85.5	18.27	67.23	-85.5
Average	88.04	-2.54	-85.5	88.15	-2.65	-85.5
Experimental	18.3	6.6	-24.9	20.4	-5.3	-15.1

quadrupole coupling constants in Table 5.9 can be compared with those based on the known monomer coupling constants[50] and the structure of the complex derived above. The principal coupling constant of D_2CO is 171 kHz[50] and is assumed to be along the C-D bond. The deuterium nuclear quadrupole coupling constants in Ne-D_2CO are found by projecting the monomer constant along the C-D onto the principal inertial axes of the Ne-D_2CO complex. The projections are given by equation 5.1:

$$\chi_{mm} = \chi_0 \left\langle P_2(\cos\theta_m) \right\rangle;\ m = a,b,c \qquad (5.1)$$

Here, χ_0 is the monomer coupling constant of 171 kHz and θ_m is the angle between the C-D bond and the m-principal axis. The brackets $\langle\rangle$ indicate averaging over the large amplitude motions.

The observed deuterium nuclear quadrupole coupling constant for a given axis is an average of two deuterium nuclear coupling constants due to the fact that Ne-D_2CO has two equivalent deuterium nuclei. The angles of the C-D bonds with the a- and b-axes are virtually identical for ^{20}Ne-D_2CO and ^{22}Ne-D_2CO. The two C-D bonds have angles of

12.9° and 50.6° with the a-axis. The angles formed with the b-axis are just 90° less those angles formed with the a-axis. Shown in Table 5.9 are the calculated deuterium nuclear quadrupole coupling constants for the Ne-D_2CO ground tunnelling state complexes as well as the experimental constants for comparison. The individual constants for each deuterium nucleus as well as an average nuclear quadrupole coupling constant are tabulated.

The surprisingly good agreement of calculated and experimental χ_{bb} values, and the discrepancy between experimental and calculated χ_{aa} and χ_{cc} values are a result of the large amplitude motion of the formaldehyde subunit within the complex. This motion is a rotation of formaldehyde about its C_2 axis. Since this C_2 axis is nearly parallel to the b-axis of the complex, the large amplitude motion does not affect the χ_{bb} of the complex significantly. However, this motion leads to an averaging of calculated χ_{aa} and χ_{cc} values. As with Ar-D_2CO, the value of χ_{cc} is smaller than the χ_{cc} value of the formaldehyde monomer (-85.5 kHz) in Ne-D_2CO. The experimental χ_{cc} values correspond to average angles of 60.9° and 58.4° of the c-axis of formaldehyde with the complex c-axis for ^{20}Ne-D_2CO and ^{22}Ne-D_2CO, respectively. These values were evaluated using Equation 5.1. The corresponding average dihedral angles are 29.1° and 31.6° for ^{20}Ne-D_2CO and ^{22}Ne-D_2CO, respectively. These average dihedral angles are roughly 10° larger then the average dihedral angles of Ar-D_2CO in the ground and first excited tunnelling states. These result are not unexpected because the interaction of formaldehyde with neon is significantly weaker as a result of the lower polarizability of neon as compared to argon.

5.5 CONCLUSIONS

The ground tunnelling state of the Ne-H_2CO van der Waals complex has been identified using the deuterium nuclear quadrupole hyperfine structure of the Ne-D_2CO isotopomers. The *ab initio* structure, to be presented in Chapter six of this thesis, agrees reasonable well with the derived structure. The deuterium nuclear quadrupole coupling constants χ_{aa}, $_{abb}$, and χ_{cc} add additional proof that the tunnelling motion is an internal rotation about the C_2 axis of the formaldehyde subunit. Additionally, the large amplitude motions of the neon atom in the complex are larger than those of the Ar-H_2CO complex as demonstrated by the χ_{cc} coupling constant.

CHAPTER SIX

AB INITIO CALCULATIONS ON Ne-H_2CO

6.1 INTRODUCTION

The ultimate goal in the study of intermolecular interactions is the construction of an accurate potential energy surface that can reproduce experiment results. One approach is to construct an *ab initio* potential energy surface and then to scale or morph[59] it until spectroscopic data can be reproduced with sufficient accuracy. *ab initio* calculations have also been used to provide equilibrium geometries of van der Waals complexes as starting points for spectroscopic searches and assignments. More recently, computer codes have become available that can determine the bound energy levels of a complex that are supported by, for example, an *ab initio* potential energy surface.[3,4,5] The combination of *ab initio* calculations and bound states determination was used in the investigation of the He-OCS complex.[60] This complex is so floppy that the usual semi-rigid rotor approach of assuming a structure and calculating the rotational constants is totally inadequate.

6.2 EXPERIMENTAL

6.2.1 SUPERMOLECULAR APPROACH

Most of the interest, in the context of rotational spectroscopy of complexes, is the van der Waals interaction energy, ΔE, that is only a small fraction of the total energy of the system. In the supermolecular approach, employed in this work, a series of three calculations are done for each molecular geometry. The energies E_A of the monomer, H_2CO, and E_B of Ne, are subtracted from E_{AB}, the energy of the Ne-H_2CO dimer to yield

ΔE:

$$\Delta E = E_{AB} - E_A - E_B \qquad (6.1)$$

6.2.2 COUNTERPOISE CORRECTION

It has been shown that the monomer energies, E_A and E_B can be significantly lowered if the basis set of the other respective monomer is included in the calculation. In other words, each monomer can borrow basis set functions from the other to lower the energy.[61,62] This basis set superposition error[61] is accounted for by applications of the counterpoise correction.[33] E_A and E_B are calculated in the presence of the basis functions for B or A, respectively. These basis functions are centred at the location of the monomer in the particular dimer geometry at which ΔE is being determined. Some controversy has existed as to the method that should be used in the counterpoise correction and whether the counterpoise correction overcorrects the base set superposition error. Such arguments have been put to rest, because proof has been given that the counterpoise corrections does not overcorrect the basis set superposition error. Hence, the full dimer basis set should be used in calculating the counterpoise correction.[62]

6.3 BASIS SETS

6.3.1 ATOMIC BASIS SETS

The calculations done on Ne-H_2CO used Sadlej's pVTZ[27] basis set for H, C and O. This basis set was used for two reasons. Firstly, this basis set was used in the calculations of Ar-H_2CO[49] and the use of this basis set for Ne-H_2CO will allow meaningful

comparisons between the calculations on Ar-H_2CO and Ne-H_2CO. Secondly, this basis set has been shown to be well suited 'for the calculation of molecular interaction potentials.'[27] The basis set used for neon is Dunning's aug-cc-pVTZ,[26] since there is no basis set for neon included in Sadlej's pVTZ basis set. Dunning's basis set was chosen because it contains high angular functions that are necessary for calculations on van der Waals complexes. High angular functions, d, f and higher, are required to properly account for the dispersion part of the interaction energy. In van der Waals complexes, the dispersion interaction is often the major contributor to the interaction energy.

6.3.2 BOND FUNCTIONS

The calculations on Ne-H_2CO include the use of bond functions to achieve a more complete dimer basis set description at reduced computational cost.[29] A simplistic view of how bond functions work is as follows. Basis functions are broken down into several different classifications, s, p, d, f, etc. Each classification represents a different type of atomic orbital and has a different number of basis functions, one for s, three for p, five for d, seven for f and so on. Now for argument sake, take two atoms and place a p function on each one to represent a bond between the two atoms.[63] The total number of basis functions will be six, three for each p function. Now look at the two p functions that make the bond between the two atoms. The two p orbitals will look approximately spherical, resembling s orbitals. Now remove the two p functions on the two atoms and place two s functions between the two atoms in the middle. An s function requires only one basis function and the s functions resemble the two lobes of the p functions that are

involved in bond formation, but the computational cost savings is four basis functions. This shows how bond functions achieve a more complete basis set description at reduced computational cost.

The bond functions used in the calculation of Ne-H_2CO were 3s3p2d with exponents of $\alpha_{s,p}$=0.9, 0.3, 0.1 and α_d= 0.6, 0.2.[29] The value of the exponents of the bond functions are not critical[29] for their use to improve the calculations. The bond functions should be placed approximately at the centre of the bond. However, the exact position of the bond functions is not very crucial..[30,64]

6.3.3 GEOMETRIES

The geometry used for the formaldehyde monomer was the geometry optimized by the GAUSSIAN 94 program[25] using the Møller-Plesset fourth order perturbation theory[23] with Sadlej's pVTZ basis set. The geometry of H_2CO was froze in all calculations, since the rotational spectra measured were all in the ground vibrational state.

The calculations of Ne-H_2CO can be broken down into three different coordinates along which calculations can be carried out. The first coordinate, R, is a radial coordinate defined by the distance from the centre of mass of the formaldehyde monomer in the complex to the neon atom. The second coordinate, θ, is the angle formed by carbon, the formaldehyde monomer's centre of mass and the neon atom. The last coordinate, Φ, is the dihedral angle formed between the plane of the formaldehyde monomer and the plane defined by the three heavy atoms in the complex (O, C, and Ne). The three coordinates for this calculation form a three dimensional potential energy surface. The calculations

along the radial coordinate start at 2.50Å and go to 10.00Å. The interval between calculations along the radial coordinate are uneven in order to accurately reflect the potential minimum along a given theta coordinate. A total of 12 different radial values were calculated at each angle θ and Φ.

The potential energy surface of the Ne-H_2CO has certain elements of symmetry that reduce the number of calculations required. The θ component need only be calculated from 0° to 180° as the angles 180° to 360° are just a reflection of the calculations from 0° to 180°. The dihedral coordinate (Φ) need only be calculated from 0° to 90° as the other three quadrants are equivalent. The calculations along the θ coordinate were done from θ = 0° to 180° in 20° intervals. The calculations along the dihedral coordinate (Φ) were done from Φ = 0° to 90° in 15° intervals. In total, 696 points on the multidimensional potential energy surface were calculated. When the dihedral coordinate is non-zero and the θ coordinate is 0° or 180°, the value is the same as if the dihedral angle was 0°. In total, along with the counterpoise correction, 2088 individual calculations were performed.

6.4 RESULTS AND DISCUSSION

6.4.1 GLOBAL MINIMUM

The calculated potential energy points after the counterpoise correction are given in Table 6.1. The global minimum is located at R = 3.50Å, θ = 100° and Φ = 0°. The depth of the potential energy surface at the global minimum is -344.81μH. A representation of the potential energy surface at a dihedral angle of 0° is shown in Figure

Table 6.1: Calculated *ab initio* Energies[a] on the Multidimensional Potential Energy Surface of Ne-H_2CO using Møller-Plesset Fourth Order Perturbation Theory.

R[b] / θ[c] (°)	2.50	3.00	3.50	3.80	4.20	4.40	4.60	4.80	5.20	6.60	8.00	10.00
						Φ = 0°						
0	82394.97	11075.36	664.12	-208.85	-295.58	-245.36	-192.64	-147.81	-86.26	-16.95	-4.38	-0.98
20	135415.31	21080.96	2399.56	376.02	-166.53	-188.08	-169.46	-140.28	-87.82	-17.45	-4.46	-0.98
40	175590.14	28378.13	3749.62	857.84	-49.29	-131.04	-142.05	-127.32	-85.16	-17.18	-4.36	-0.94
60	74790.96	12444.14	1457.92	201.99	-139.43	-149.95	-133.94	-110.98	-70.03	-14.22	-3.71	-0.84
80	14917.31	1684.66	-144.37	-235.55	-177.59	-141.22	-110.12	-85.20	-50.99	-10.57	-2.99	-0.72
100	4411.56	-118.36	-344.81	-255.86	-152.41	-116.07	-88.48	-67.71	-40.19	-8.37	-2.57	-0.66
120	8800.05	571.00	-236.69	-222.02	-147.09	-114.55	-88.31	-67.87	-40.18	-8.00	-2.55	-0.68
140	18841.35	1763.28	-149.84	-226.72	-166.87	-131.89	-102.17	-78.37	-45.81	-8.64	-2.76	-0.74
160	29722.14	2748.32	-138.60	-262.24	-194.40	-152.81	-117.66	-89.68	-51.64	-9.35	-2.98	-0.80
180	34498.18	3094.40	-153.28	-285.25	-208.33	-162.62	-124.41	-94.25	-53.70	-9.61	-3.06	-0.82
						Φ = 15°						
0	82394.97	11075.36	664.12	-208.85	-295.58	-245.36	-192.64	-147.81	-86.26	-16.95	-4.38	-0.98
20	128489.95	19927.18	2223.85	322.21	-176.18	-191.59	-170.35	-140.15	-87.26	-17.30	-4.43	-0.98
40	153964.03	25213.27	3289.84	719.52	-71.61	-138.09	-142.97	-126.04	-83.20	-16.69	-4.27	-0.93
60	64862.21	10728.58	1202.80	129.44	-148.76	-151.37	-132.44	-108.72	-68.11	-13.79	-3.63	-0.82
80	13329.93	1418.73	-175.32	-239.73	-174.51	-137.99	-107.32	-82.98	-49.74	-10.34	-2.94	-0.72
100	4317.94	-116.93	-338.60	-251.27	-149.79	-114.18	-87.12	-66.74	-39.71	-8.27	-2.55	-0.67
120	8667.26	550.65	-238.49	-221.72	-146.39	-113.96	-87.87	-67.55	-40.02	-7.96	-2.54	-0.68
140	18550.85	1713.35	-157.70	-228.94	-167.02	-131.81	-102.01	-78.22	-45.72	-8.63	-2.76	-0.73
160	29548.54	2720.57	-142.99	-263.58	-194.58	-152.83	-117.61	-89.62	-51.60	-9.34	-2.97	-0.81
180	34498.18	3094.40	-153.28	-285.25	-208.33	-162.62	-124.41	-94.25	-53.70	-9.61	-3.06	-0.82
						Φ = 30°						
0	82394.97	11075.36	664.12	-208.85	-295.58	-245.36	-192.64	-147.81	-86.26	-16.95	-4.38	-0.98
20	111114.01	16979.58	1771.48	183.69	-200.98	-200.51	-172.46	-139.57	-85.67	-16.95	-4.36	-0.96
40	109353.19	18039.12	2219.09	398.52	-125.44	-155.66	-145.54	-123.08	-78.77	-15.79	-4.08	-0.91

Table 6.1 (continued).

R[b] / θ[c] (°)	2.50	3.00	3.50	3.80	4.20	4.40	4.60	4.80	5.20	6.60	8.00	10.00
60	44175.99	7051.32	652.14	-25.66	-166.59	-152.20	-127.23	-102.14	-63.07	-12.90	-3.45	-0.80
80	9910.49	855.87	-236.46	-245.37	-166.24	-129.87	-100.45	-77.54	-46.62	-9.80	-2.81	-0.69
100	4118.15	-108.20	-322.88	-240.16	-143.59	-109.68	-83.90	-64.44	-38.51	-8.03	-2.48	-0.64
120	8294.72	490.92	-244.99	-221.76	-144.86	-112.59	-86.80	-66.76	-39.60	-7.87	-2.51	-0.66
140	17753.59	1574.98	-179.77	-235.25	-167.52	-131.61	-101.61	-77.83	-45.49	-8.58	-2.74	-0.73
160	29074.39	2644.19	-155.03	-267.24	-195.06	-152.85	-117.46	-89.44	-51.50	-9.33	-2.96	-0.79
180	34498.18	3094.40	-153.28	-285.25	-208.33	-162.62	-124.41	-94.25	-53.70	-9.61	-3.06	-0.82
						Φ = 45°						
0	82394.97	11075.36	664.12	-208.85	-295.58	-245.36	-192.64	-147.81	-86.26	-16.95	-4.38	-0.98
20	90521.02	13397.00	1214.84	13.05	-231.22	-211.11	-174.65	-138.45	-83.49	-16.51	-4.27	-0.96
40	68667.99	10928.86	1126.48	72.17	-177.53	-171.00	-145.86	-118.06	-73.08	-14.76	-3.87	-0.88
60	26006.61	3737.54	156.55	-159.96	-176.86	-148.18	-118.83	-93.42	-57.00	-11.89	-3.24	-0.76
80	6833.65	371.64	-279.29	-243.21	-155.32	-120.09	-92.46	-71.31	-43.03	-9.20	-2.67	-0.67
100	3945.88	-89.16	-304.17	-227.64	-136.79	-104.74	-80.33	-61.86	-37.15	-7.78	-2.41	-0.62
120	7763.91	400.74	-256.83	-223.37	-143.40	-111.12	-85.54	-65.80	-39.06	-7.76	-2.47	-0.66
140	16657.27	1381.95	-211.06	-244.36	-168.34	-131.40	-101.10	-77.30	-45.15	-8.55	-2.72	-0.73
160	28427.22	2538.83	-171.64	-272.25	-195.70	-152.90	-117.27	-89.20	-51.37	-9.32	-2.97	-0.80
180	34498.18	3094.40	-153.28	-285.25	-208.33	-162.62	-124.41	-94.25	-53.70	-9.61	-3.06	-0.82
						Φ = 60°						
0	82394.97	11075.36	664.12	-208.85	-295.58	-245.36	-192.64	-147.81	-86.26	-16.95	-4.38	-0.98
20	72936.88	10267.22	721.91	-138.37	-257.55	-219.95	-176.06	-137.03	-81.33	-16.11	-4.19	-0.94
40	41671.54	5984.23	349.94	-158.00	-210.55	-178.12	-142.96	-112.10	-67.77	-13.85	-3.68	-0.85
60	14845.78	1686.58	-142.44	-234.60	-177.07	-140.90	-110.04	-85.38	-51.73	-10.99	-3.06	-0.73
80	4965.68	103.15	-292.10	-234.10	-144.99	-111.58	-85.79	-66.20	-40.08	-8.67	-2.56	-0.64
100	3851.82	-66.25	-287.95	-217.35	-131.41	-100.83	-77.47	-59.76	-35.96	-7.57	-2.35	-0.61
120	7209.37	302.51	-271.28	-226.39	-142.52	-109.95	-84.45	-64.86	-38.48	-7.68	-2.44	-0.64
140	15554.13	1184.93	-243.47	-253.90	-169.22	-131.20	-100.55	-76.73	-44.82	-8.51	-2.71	-0.72

Table 6.1 (continued).

R[b] / θ[c] (°)	2.50	3.00	3.50	3.80	4.20	4.40	4.60	4.80	5.20	6.60	8.00	10.00
160	27780.92	2432.50	-188.41	-277.25	-196.29	-152.91	-117.09	-89.00	-51.23	-9.31	-2.96	-0.79
180	34498.18	3094.40	-153.28	-285.25	-208.33	-162.62	-124.41	-94.25	-53.70	-9.61	-3.06	-0.82
						Φ = 75°						
0	82394.97	11075.36	664.12	-208.85	-295.58	-245.36	-192.64	-147.81	-86.26	-16.95	-4.38	-0.98
20	61670.16	8228.74	397.14	-238.23	-274.52	-225.38	-176.68	-135.86	-79.77	-15.84	-4.15	-0.94
40	27558.89	3332.56	-70.38	-280.53	-225.87	-179.77	-139.62	-107.49	-64.08	-13.24	-3.56	-0.84
60	9441.22	700.47	-279.15	-264.62	-173.43	-134.52	-103.63	-79.89	-48.31	-10.41	-2.94	-0.70
80	4104.13	-4.12	-289.57	-224.73	-137.74	-106.00	-81.58	-63.04	-38.24	-8.33	-2.48	-0.62
100	3815.23	-48.89	-277.13	-210.75	-128.20	-98.52	-75.76	-58.43	-35.12	-7.43	-2.31	-0.60
120	6788.99	226.56	-283.19	-229.39	-142.19	-109.23	-83.63	-64.11	-37.99	-7.63	-2.42	-0.64
140	14742.65	1038.44	-267.89	-261.15	-169.87	-131.00	-100.09	-76.28	-44.56	-8.48	-2.70	-0.73
160	27308.48	2354.11	-200.75	-280.90	-196.72	-152.90	-116.92	-88.80	-51.14	-9.30	-2.96	-0.79
180	34498.18	3094.40	-153.28	-285.25	-208.33	-162.62	-124.41	-94.25	-53.70	-9.61	-3.06	-0.82
						Φ = 90°						
0	82394.97	11075.36	664.12	-208.85	-295.58	-245.36	-192.64	-147.81	-86.26	-16.95	-4.38	-0.98
20	57847.40	7531.20	285.27	-272.64	-280.26	-227.16	-176.82	-135.39	-79.21	-15.74	-4.11	-0.93
40	23288.07	2521.28	-198.94	-317.48	-230.04	-179.85	-138.26	-105.78	-62.78	-13.04	-3.52	-0.82
60	7879.33	418.89	-316.52	-271.88	-171.54	-132.03	-101.30	-77.96	-47.14	-10.21	-2.88	-0.69
80	3868.06	-29.68	-286.85	-220.90	-135.15	-104.05	-80.17	-62.00	-37.63	-8.20	-2.44	-0.61
100	3806.71	-42.59	-273.32	-208.48	-127.18	-97.80	-75.21	-57.98	-34.80	-7.37	-2.30	-0.60
120	6632.11	198.03	-287.79	-230.67	-142.14	-108.99	-83.33	-63.82	-37.78	-7.62	-2.41	-0.65
140	14444.78	984.38	-276.98	-263.86	-170.09	-130.90	-99.90	-76.08	-44.45	-8.47	-2.70	-0.72
160	27135.70	2325.32	-205.28	-282.23	-196.86	-152.90	-116.87	-88.73	-51.10	-9.30	-2.97	-0.79
180	34498.18	3094.40	-153.28	-285.25	-208.33	-162.62	-124.41	-94.25	-53.70	-9.61	-3.06	-0.82

[a] - The results are shown in μH after the counterpoise correction.

[b] - Radial coordinate in Angstroms (Å).

[c] - The θ coordinate is defined as the angle formed by formaldehyde's carbon, formaldehyde's centre of mass and the neon atom.

6.1. The large repulsive area on the potential energy surface is the area where the neon atom is close to the hydrogen atom.

The multidimensional potential energy surface has revealed three local minima. The locations of the local minima in terms of R, θ, and Φ are: (4.20Å, 0°, 0°), (3.80Å, 180°, 0°), and (3.80Å, 40°, 90°). The energies of the local minima are -295.58μH, -285.25μH, and -317.48μH, respectively. Clearly, the local minimum at $\Phi = 90°$ has the lowest depth.

6.4.2 TUNNELLING PATHWAYS

The multidimensional potential energy surface can be used to determine more subtle features of the complex other than their structures. Assuming that the internal dynamics of Ne-H_2CO is qualitatively similar to that of Ar-H_2CO,[49] a tunnelling motion can occur that interchanges the two equivalent hydrogen atoms.

The three possible tunnelling pathways are represented in Figure 6.2 and Figure 6.3. Figure 6.2 represents the in-plane minimum energy pathways. One motion of the neon atom is around the oxygen atom of the formaldehyde, the other motion is around the carbon atom of formaldehyde. Figure 6.3 represents the out of plane minimum energy pathway. The out of plane motion is the movement of the neon atom out of the plane formed by the formaldehyde monomer to the equivalent position. The minimum energy pathways as determined from the *ab initio* potential energy surface are plotted in Figures 6.2 and 6.3 for the in-plane and out-of-plane tunnelling pathways, respectively. In both the in-plane and out-of-plane tunnelling pathways are secondary potential energy minima.

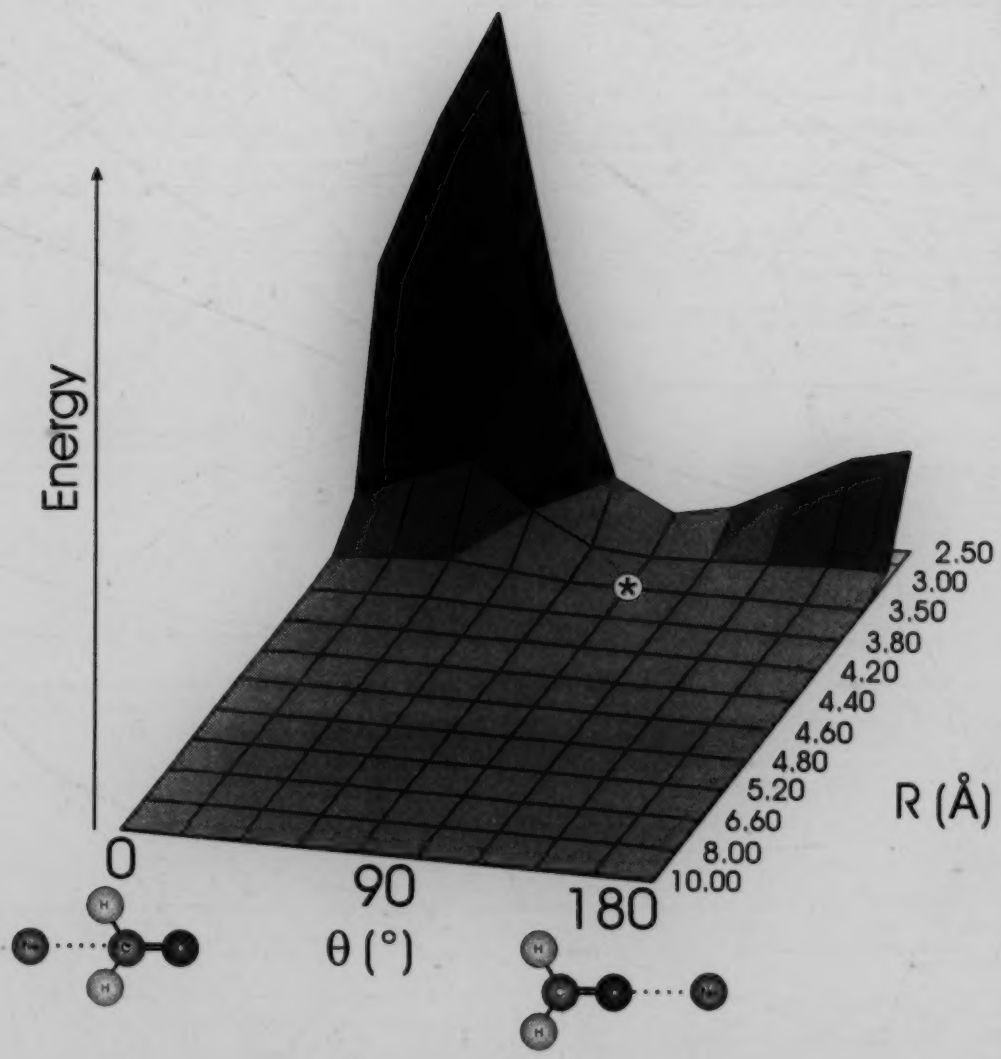

Figure 6.1: The potential energy surface of Ne-H_2CO at a dihedral angle of $\Phi = 0°$. The θ coordinate is the angle defined by the carbon atom, formaldehyde's centre of mass and the neon atom. The calculation of this potential energy surface was carried out at the Møller-Plesset fourth order perturbation theory level with counterpoise correction. The global minimum is a planar configuration ($\Phi = 0°$), at R = 3.50Å and $\theta = 100°$. The global minimum is indicated on the potential energy surface with ⊛. The energy at the minimum is -344.8μH. The strongly repulsive area on potential energy surface corresponds to the area around the hydrogens of the formaldehyde monomer.

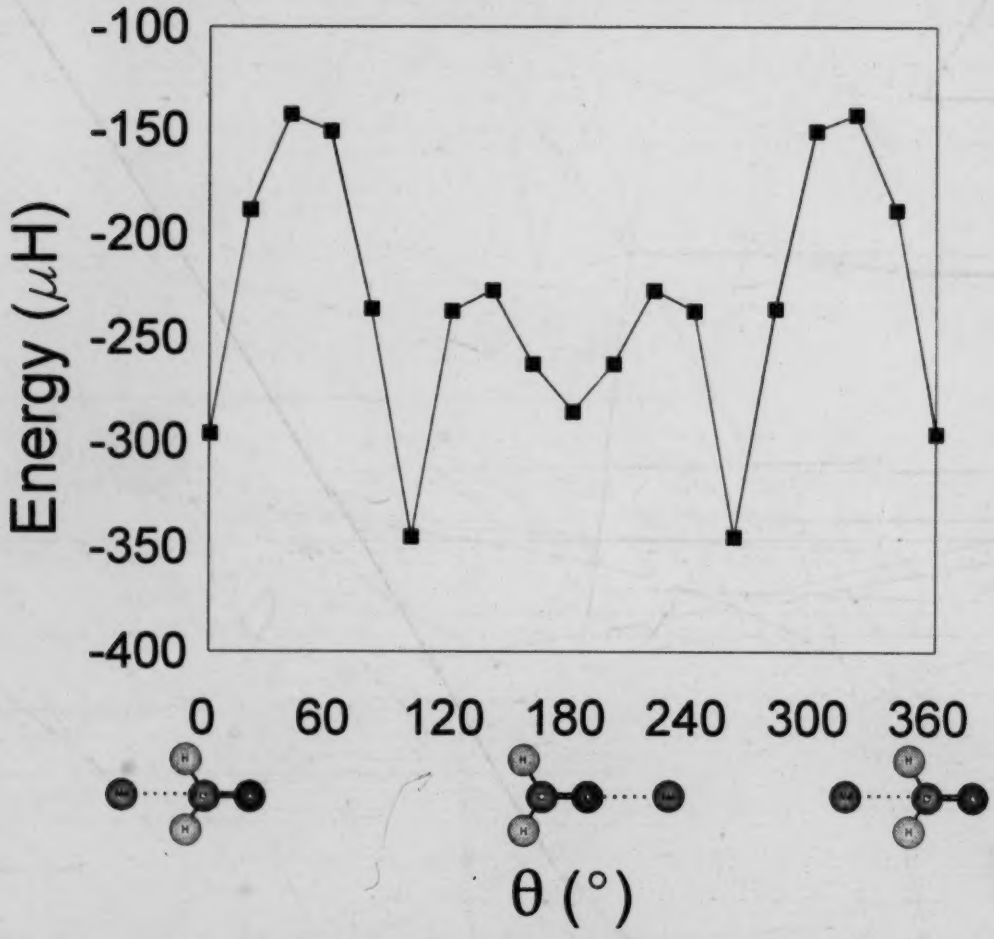

Figure 6.2: The tunnelling pathways in Ne-H_2CO for the in-plane motions is shown above. The points at $\theta = 0°$ and $\theta = 360°$ are equivalent. The global minimum at $\theta = 100°$ also occurs at the equivalent geometry of $\theta = 260°$. Also shown in this figure are two secondary (local) minima at $\theta = 0°/360°$ and $\theta = 180°$. The local minimum at $0°/360°$ corresponds to the position of the neon atom between the hydrogen atoms near the carbon atom of formaldehyde and the minimum at 180° corresponds to the neon atom being at the oxygen end of the formaldehyde monomer.

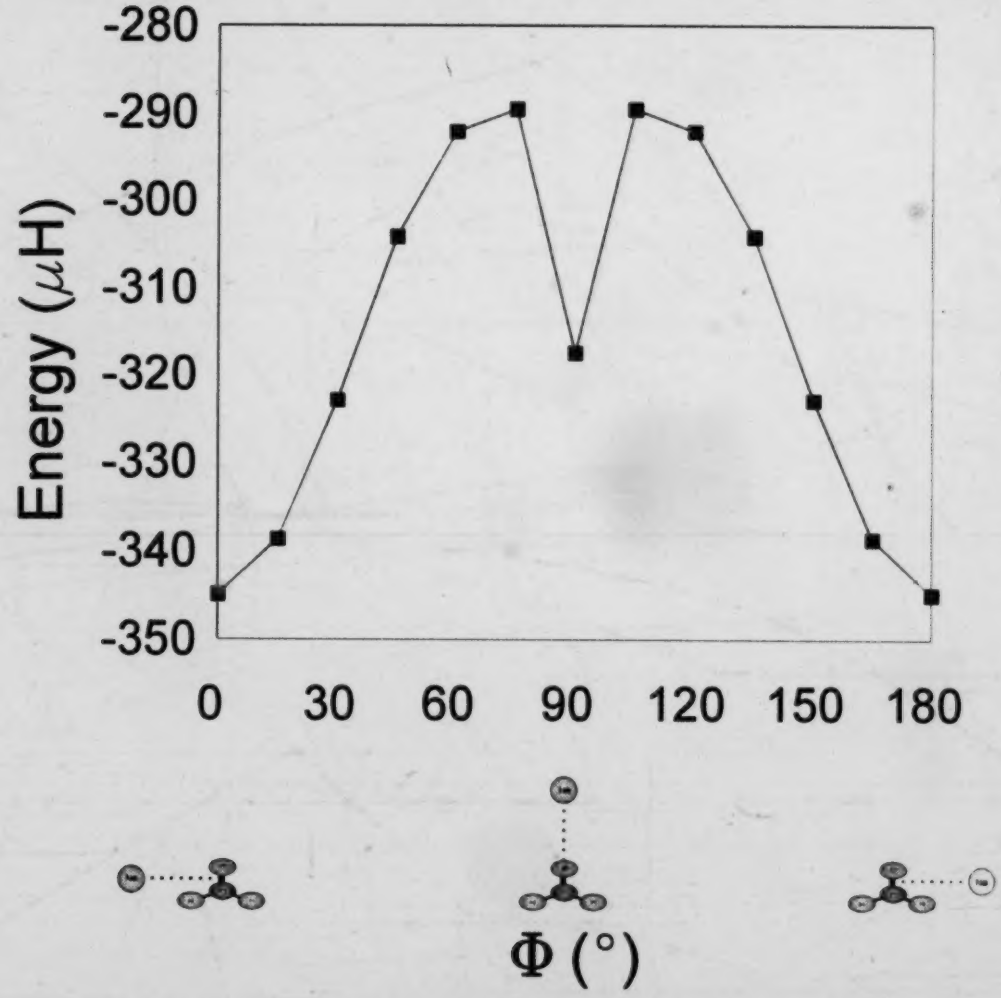

Figure 6.3: The tunnelling pathway in Ne-H_2CO for the out of plane motion is shown above. The neon positions at 0° and 180° are equivalent. A local minimum at the dihedral angle of 90° is seen in the figure. This minimum corresponds to the neon atom sitting above the plane of the formaldehyde monomer.

Table 6.2: Barriers[a] to the Tunnelling Motions in Ne-H_2CO.

Motion	Local minimum	Barrier Height	Barrier[b]
In-Plane			
Around C atom	-295.58	-142.05	202.76
Around O Atom	-285.25	-226.72	118.09
Out of Plane	-317.48	-289.57	55.24

[b] - all energies in μH.
[a] - from global minimum of -344.81μH.

Listed in Table 6.2 are the various local minima determined from Figures 6.2 and 6.3 and the barriers associated with each tunnelling motion. The preferred motion is the out of plane pathway with a barrier of 55.24μH. The barrier to this pathway is half that of the next lowest barrier, that of the in-plane tunnelling motion of the neon atom moving around the oxygen atom of the formaldehyde monomer with a barrier of 118.09μH.

In order to evaluate the feasability of the out of plane tunnelling motion, it is important to determine the change of the radial coordinate and the change in the θ coordinate during this motion. For the out of plane motion, the radial component starts at 3.50Å and maintains that value until it reaches the local minimum at the dihedral angle of 90° where the radial coordinate changes to 3.80Å. This corresponds to an amplitude of 0.30Å for the radial coordinate during this motion. The angular amplitude also changes during the tunnelling motion. The tunnelling motion starts at θ = 100° and changes to θ = 80° at a dihedral angle of 60°. This corresponds to an angular amplitude 20° during the tunnelling motion.

6.5 CONCLUSIONS

When comparing the present *ab initio* calculations on Ne-H_2CO with the *ab initio* calculations on Ar-H_2CO,[49] one finds that the distance from the centre of mass of the formaldehyde monomer changes from 3.75Å to 3.50Å when going from argon to neon. The experimental value for Ar-H_2CO is 3.638Å. The discrepancy between the calculated value and the experimental value can be attributed in part to the relatively large spacing of the *ab initio* points of 0.25Å. Furthermore, it must be kept in mind that the *ab initio* value is an equilibrium value, whereas the experimental value is an effective value, averaged over the large amplitude vibrational motions. Nevertheless, the *ab initio* value in Ar-H_2CO agrees with the experimental value with the error of the potential energy surface.

The *ab initio* points calculated for Ne-H_2CO are clustered around the minimum energy to get a more accurate picture of where the minimum is. The calculated potential energy surface of Ne-H_2CO was calculated in the same manner as the potential energy surface of Ar-H_2CO, so it is reasonable to expect that the location of the neon atom in the Ne-H_2CO complex will be close to 3.50Å.

Three possible tunnelling pathways in Ne-H_2CO are mapped out on the *ab initio* potential energy surface. The out of plane tunnelling pathway is the preferred pathway as its barrier to internal rotation is half that of the next nearest tunnelling pathway. The radial components for this pathway does change by 0.30Å and the angular amplitude is on the order of 20°.

CHAPTER SEVEN

CONCLUSIONS

Many conclusions can be reached from the findings of this thesis. The molecular symmetry group analysis clearly shows that there are two tunnelling states for all Rg-H_2CO van der Waals complexes, the ground tunnelling state and the first excited tunnelling state which is metastable. Also from the molecular symmetry group analysis, a specific set of nuclear spin states of Rg-D_2CO is associated with a given tunnelling state. Nuclear spin states 0 and 2 are associated with the ground tunnelling state, while nuclear spin state 1 is associated with the first excited tunnelling state.

The previous study by Novick[10] on Ar-H_2CO and Ar-D_2CO was corrected with respect to Ar-D_2CO. The deuterium hyperfine structure of deuterated formaldehyde in the Ar-D_2CO complex allowed the unambiguous assignment of the two tunnelling states. The inertia defect of Ar-D_2CO suggests that there are large amplitude motions going on within the complex. This is supported by the deuterium nuclear quadrupole coupling constants. The calculated nuclear quadrupole coupling constants from the structure suggests that there is some averaging along the a-axis and c-axis when they are compared with the experimental nuclear quadrupole coupling constants. Averaging about the c-axis is an out of plane motion.

The structures of Ne-H_2CO and Ne-D_2CO were not well determined. The $K_a = 0$ transitions were found, but the confidence in the $K_a = 1$ transitions is low. The floppiness of the Ne-H_2CO complexes is evident by the centrifugal distortion constant Δ_J, which is an order of magnitude larger then the centrifugal distortion constant in Ar-H_2CO. The

determined deuterium nuclear quadrupole coupling constant of Ne-D_2CO, χ_{aa} is smaller then the χ_{aa} nuclear quadrupole coupling constant of Ar-D_2CO. With Ar-D_2CO, the calculated nuclear quadrupole coupling constant, χ_{aa}, is larger than the experimental nuclear quadrupole coupling constant. This can be interpreted to mean that there is some averaging (motion) about the a-axis and with the χ_{aa} value smaller in Ne-D_2CO than in Ar-D_2CO, the averaging about the a-axis must be much larger.

To help understand what is happening with the neon formaldehyde complexes, the *ab initio* calculations added insight into these complexes. The calculations shows that the equilibrium structure should be a planar complex. The internal rotation of the formaldehyde monomer in the complex is determined to be a rotation of the formaldehyde about its C_2 axis. The barrier to internal rotation about formaldehyde's C_2 axis is half that of the next nearest barrier to internal rotation. In the internal rotation, the radial amplitude changes by 0.30Å and the angular amplitude changes by 20°. These radial and angular amplitudes will influence the determined ground state structure of the Ne-H_2CO complex. This will be evident by having relatively large centrifugal distortion constants.

The work carried out in this thesis can be further extended by the complete determination of the Ne-H_2CO and Ne-D_2CO structures. The use of such programs as BOUND[5] could be very useful in the spectral search for transitions of the Ne-H_2CO complexes. The large centrifugal distortion constant Δ_J is an indication of the floppiness of this complex and the spectra assignment could be helped with such computer programs as BOUND.

BIBLIOGRAPHY

1. M. Rigby, E.B. Smith, W.A. Wakeham and G.C. Maitland, in "The Forces Between Molecules", Oxford University Press, Oxford, 1986.

2. A.J. Stone, in "The Theory of Intermolecular Forces", Oxford University Press, Oxford, 1996.

3. R.C. Cohen and R.J. Saykally, J. Chem. Phys. **95**, 7891 (1991).

4. R.C. Cohen and R.J. Saykally, J. Chem. Phys. **98**, 6007 (1993).

5. J.M. Hutson, BOUND computer code, version 5, Coll. Comp. Proj. No. 6 (1993).

6. T. Oka, H. Hirakawa and K. Shimoda, J. Phys. Soc. Japan. **15**, 2265 (1960).

7. T. Oka, J. Phys. Soc. Japan. **15**, 2274 (1960).

8. K. Takagi and T. Oka, J. Phys. Soc. Japan. **18**, 1174 (1963).

9. M.D. Harmony, V.W. Laurie, R.L. Kuczkowski, R.H. Schwendeman, D.A. Ramsay, F.J. Lovas, W.J. Lafferty, and A.G. Maki, J. Phys. Chem. Ref. Data. **8**, 619 (1979).

10. S.E. Novick, J. Chem. Phys. **99**, 7506 (1993).

11. Y. Xu and W. Jäger, J. Chem. Phys. **106**, 7968 (1997).

12. J. Ekkers and W.H. Flygare, Rev. Sci. Instrum. **47**, 448 (1976).

13. T.J. Balle and W.H. Flygare, Rev. Sci. Instrum. **52**, 33 (1981).

14. J.-U. Grabow and W. Stahl, Z. Naturforsch. **45a**, 1043 (1990).

15. T.A. Miller, Science **223**, 545 (1984).

16. D.R. Miller, in "Atomic and Molecular Beam Methods" (G. Scoles, Ed), Vol 1, Ch. 2, Oxford University Press, New York, 1988.

17. D.H. Levy, Ann. Rev. Phys. Chem. **31**, 197 (1980)

18. R.E. Smalley, L. Wharton and D.H. Levy, J. Chem. Phys. **63**, 4977, (1975).

19. J.C. McGurk, T.G. Schmalz and W.H. Flygare, Adv. Chem. Phys. **25**, 1 (1974).

20. H. Dreizler, Mol. Phys. **59**, 1 (1986).

21. H. Dreizler, Ber. Bunsenges. Phys. Chem. **99**, 1451 (1995).

22. F. Bloch, Phys. Rev. **70**, 460 (1946).

23. C.H.R. Møller and M.S. Plesset, Phys. Rev. **46**, 618 (1934).

24. Gaussian 94, Revision D.3, M.J. Frisch, G.W. Trucks, H.B. Schlegel, P.M.W. Gill, B.G. Johnson, M.A. Robb, J.R. Cheeseman, T. Keith, G.A. Petersson, J.A. Montgomery, K. Raghavachari, M.A. Al-Laham, V.G. Zakrzewski, J.V. Ortiz, J.B. Foresman, J. Cioslowski, B.B. Stefanov, A. Nanayakkara, M. Challacombe, C.Y. Peng, P.Y. Ayala, W. Chen, M.W. Wong, J.L. Andres, E.S. Replogle, R. Gomperts, R.L. Martin, D.J. Fox, J.S. Binkley, D.J. Defrees, J. Baker, J.P. Stewart, M. Head-Gordon, C. Gonzalez, and J.A. Pople, Gaussian, Inc., Pittsburgh PA, 1995. This software is for Linux based operating systems.

25. Gaussian 94, Revision E.3, M.J. Frisch, G.W. Trucks, H.B. Schlegel, P.M.W. Gill, B.G. Johnson, M.A. Robb, J.R. Cheeseman, T. Keith, G.A. Petersson, J.A. Montgomery, K. Raghavachari, M.A. Al-Laham, V.G. Zakrzewski, J.V. Ortiz, J.B. Foresman, J. Cioslowski, B.B. Stefanov, A. Nanayakkara, M. Challacombe, C.Y. Peng, P.Y. Ayala, W. Chen, M.W. Wong, J.L. Andres, E.S. Replogle, R. Gomperts, R.L. Martin, D.J. Fox, J.S. Binkley, D.J. Defrees, J. Baker, J.P. Stewart, M. Head-Gordon, C. Gonzalez, and J.A. Pople, Gaussian, Inc., Pittsburgh PA, 1995. This software is for Microsoft Windows based operating systems.

26. T.H. Dunning, Jr., J. Chem. Phys. **90**, 1007 (1989).

27. A.J. Sadlej, Coll. Czech. Chem. Comm. **53**, 1995 (1988).

28. F.-M. Tao and Y.-K. Pan, Chem. Phys. Lett. **194**, 162 (1992).

29. F.-M. Tao and Y.-K. Pan, J. Chem. Phys. **97**, 4989 (1992).

30. F.-M. Tao, J. Chem. Phys. **98**, 3049 (1993).

31. The bond functions used were $\alpha_{s,p} = 0.9, 0.3, 0.1$ and $\alpha_d = 0.6, 0.2$.

32. J.A. Pople, Faraday Discuss. Chem. Soc. **73**, 7 (1982).

33. S.F. Boys and F. Bernardi, Mol. Phys. **19**, 553 (1970).

34. P.H. Bunker and P. Jensen, in "Molecular Symmetry and Spectroscopy", 2nd ed., NRC Research Press, Ottawa, 1998.

35. W. Pauli, Phys. Rev. **58**, 716 (1940).

36. F.A. Baiocchi and W. Klemperer, J. Chem. Phys. **78**, 3509 (1983).

37. F.J. Lovas, R.D. Suenram, S. Ross and M. Klobukowski, J. Mol. Spec. **123**, 167 (1987).

38. G.T. Fraser, C.W. Gillies, J. Zozom, F.J. Lovas, and R.D. Suenram, J. Mol. Spec. **126**, 200 (1987).

39. A.C. Legon, J. Chem. Soc. Faraday Trans. **92**, 2677 (1996)

40. E.J. Goodwin and A.C. Legon, J. Chem. Phys. **87**, 2426 (1987).

41. N.W. Howard and A.C. Legon, J. Chem. Phys. **88**, 6793 (1988).

42. F.J. Lovas, R.D. Suenram, L.H. Coudert, T.A. Blake, K.J. Grant, and S.E. Novick, J Chem. Phys. **92**, 891 (1990).

43. T.A. Blake, S.E. Novick, F.J. Lovas, and R.D. Suenram, J. Mol. Spec. **154**, 72 (1992).

44. F.J. Lovas, C.L. Lugez, J. Mol. Spec. **179**, 320 (1996).

45. S.A. Cooke, G.K. Corlett, C.M. Evans, A.C. Legon, and J.H. Holloway, J. Chem. Phys. **108**, 39 (1998).

46. J.K.G. Watson, J. Chem. Phys. **46,** 1935 (1967).

47. J.K.G. Watson, in "Vibrational Spectra and Structure." (J.R. Durig, Ed), Vol 6, Ch. 1, Elsevier Scientific Publishing Company, New York, 1977.

48. H.P. Benz, A. Bauder and Hs.H. Günthard, J. Mol. Spec. **21**, 156 (1966).

49. J. Sadlej, M.M. Szczęśniak, and G. Chałasiński, J. Chem. Phys. **99**, 5211 (1993).

50. W.H. Flygare, J. Chem. Phys. **41**, 206 (1964).

51. K.A. Walker, T. Ogata, W. Jäger, M.C.L. Gerry, and I. Ozier, J. Chem. Phys. **106**, 7519 (1997).

52. T. Ogata, W. Jäger, I. Ozier, and M.C.L. Gerry, J. Chem. Phys. **98**, 9399 (1993).

53. Y. Xu and W. Jäger, J. Mol. Spectrosc. **192**, 435 (1998).

54. J.M. Steed, T.A. Dixon and W. Klemperer, J. Chem. Phys. **79**, 4095 (1979).

55. G.T. Fraser, A.S. Pine and R.D. Suenram, J. Chem. Phys. **88**, 6157 (1988).

56. F.J. Lovas and R.D. Suenram, J. Chem. Phys. **87**, 210 (1987).

57. Y. Xu and M.C.L. Gerry, J. Mol. Spectrosc. **169**, 542 (1995).

58. J.A. Shea, W.G. Read, and E.J. Campbell, J. Chem. Phys. **79**, 2559 (1983).

59. M. Meuwly and J.M. Hutson, J. Chem. Phys. **110**, 8338 (1999).

60. K. Higgins and W. Klemperer, J. Chem. Phys. **110**, 1383 (1999).

61. B. Liu and A.D. McLean, J. Chem. Phys. **59**, 4557 (1973).

62. F.B. van Duijneveldt, J.G.C.M. van Duijneveldt-van de Rijdt, and J.H. van Lenthe, Chem. Rev. **94**, 1873 (1994).

63. F.-M. Tao, J. Mol. Struct. **367**, 55 (1996).

64. R. Burcl, G. Chałasiński, R. Bukowski and M.M. Szczęśniak, J. Chem. Phys. **103**, 1498 (1995).